

Modeling stomatal and nonstomatal effects of water deficits on CO₂ fixation in a semiarid grassland

R. F. Grant¹ and L. B. Flanagan²

Received 7 September 2006; revised 15 February 2007; accepted 29 May 2007; published 22 August 2007.

[1] The confidence with which we can model water deficit effects on grassland productivity is limited by uncertainty about the mechanisms, stomatal and nonstomatal, by which soil water deficits reduce CO₂ uptake. We propose that these reductions can accurately be modeled from a combination of stomatal effects on gaseous CO₂ diffusion and nonstomatal effects on biochemical CO₂ fixation. These effects can be combined through a solution for the intercellular CO₂ concentration (C_i) at which rates of diffusion and fixation are equal for each leaf surface in the canopy. In this model, both stomatal and nonstomatal effects are driven by a common indicator of plant water status calculated in a hydraulically-driven scheme of soil-plant-atmosphere water transfer. As part of the ecosystem model *ecosys*, this combined model simulated concurrent declines in latent heat effluxes and CO₂ influxes measured by eddy covariance during soil drying in a drought-affected semiarid grassland. At the same time, the model simulated the declines in C_i at which CO₂ fixation occurred during soil drying as calculated from seasonal measurements of phytomass $\delta^{13}\text{C}$. Alternative model formulations based on stomatal or nonstomatal effects alone simulated these declines in CO₂ influxes and in C_i less accurately than did the formulation in which these effects were combined. We conclude that modeling water deficit effects on CO₂ fixation requires the concurrent simulation of stomatal and nonstomatal effects. As part of a larger ecosystem model, this combined model can be used to assess climate effects on grassland productivity.

Citation: Grant, R. F., and L. B. Flanagan (2007), Modeling stomatal and nonstomatal effects of water deficits on CO₂ fixation in a semiarid grassland, *J. Geophys. Res.*, 112, G03011, doi:10.1029/2006JG000302.

1. Introduction

[2] The net ecosystem productivity (*NEP*) of grasslands in the Great Plains region of North America is strongly controlled by ecosystem water status which is in turn controlled by the relationship between precipitation and potential evapotranspiration (ET_p). *NEP* of these grasslands is usually positive (net C sink) during years in which precipitation exceeds ca. 0.5 ET_p and negative (net C source) during years in which it does not [e.g., Flanagan *et al.*, 2002]. Changes in *NEP* with precipitation occur because gross primary productivity (*GPP*) is comparatively more sensitive to soil water deficits than is ecosystem respiration (R_e) [Meyers, 2001; Novick *et al.*, 2004; Suyker *et al.*, 2003]. These changes are of concern because both precipitation and ET_p are believed to be changing in the Great Plains region as climate change progresses. Of particular concern would be a return to prolonged droughts during the 21st century such as are believed to have been common in western Canada before the 20th century [Sauchyn *et al.*, 2003]. Mathematical models

of terrestrial ecosystems are frequently used to predict the impacts of climate change on grassland *NEP* [e.g., Melillo *et al.*, 1996]. The reliability of such predictions depends heavily upon the accurate simulation of water deficit effects on *GPP*.

[3] There are two stages to modeling water deficit effects on *GPP*: (1) solving for the effects of ecosystem water status on canopy stomatal conductance (g_c), and (2) calculating the effects of g_c on ecosystem CO₂ uptake. There are two basic approaches to modeling water status effects on g_c . The first approach is based on the hypothesis of Schulze [1993] that abscisic acid (ABA), produced by drying root tips and transported through the xylem, causes g_c to decline. This hypothesis was developed from earlier work by Gollan *et al.* [1986], who found that declines in leaf stomatal conductance (g_l) occurred independently of leaf water potential (ψ_l). In this approach, water deficit effects on g_c are functions of soil water potential (ψ_s) or soil water content (θ) [e.g., Grünhage and Haenel, 1997]. This function may then be multiplied by functions for atmospheric effects on g_c , sometimes represented by empirical functions of photosynthetically active radiation (*PAR*), air temperature (T_a), vapor pressure deficit (D), and atmospheric CO₂ concentration (C_a) [Kimball *et al.*, 1997], but more commonly represented by a Ball-Woodrow-Berry function of D [Ball *et al.*, 1987], CO₂ fixation, and C_a [e.g., Goldberg and Bernhofer, 2001; King *et al.*, 1997; Wang and Jarvis, 1990]. In this way, soil and atmospheric water deficits interact multiplicatively on g_c . However, Tardieu and

¹Department of Renewable Resources, University of Alberta, Edmonton, Alberta, Canada.

²Department of Biological Sciences, University of Lethbridge, Lethbridge, Alberta, Canada.

Davies [1993] found that sensitivity of g_l to ABA depended on ψ_b , so that both ABA and hydraulic signals were required to model g_l robustly. Certain models [e.g., Nikolov, 1997] attempt to represent chemical (ABA) as well as hydraulic signals from roots to stomates as proposed by Tardieu and Davies [1993], but quantitative hypotheses for these signals are not yet well developed.

[4] The second approach to modeling water status effects on g_c is based on hypotheses about soil-plant-atmosphere hydraulics that allow a value for canopy water potential (ψ_c) to be found at which canopy transpiration equilibrates with root water uptake. In this approach, water deficit effects on g_c are functions of ψ_c [e.g., Tuzet *et al.*, 2003; Williams *et al.*, 1996] or turgor potential (ψ_t) [e.g., Li *et al.*, 2004; Zhang *et al.*, 2005], so that a direct effect of soil water status on g_c is not simulated. However, during soil drying, declining ψ_s and root water potentials (ψ_r) cause soil and root hydraulic resistances to rise, so that ψ_c and hence g_c decline more rapidly with rises in transpirational demand. Therefore this approach incorporates an indirect but influential soil effect when calculating g_c .

[5] For both approaches to modeling g_c , the formulation of g_c appears to be the most critical algorithm causing differences among ecosystem models in predicted fluxes of water and CO₂ [Kramer *et al.*, 2002]. However, both approaches also rely on the accurate simulation of root water uptake to calculate root zone water contents from which soil water deficit effects on g_c are derived. The modeling of root water uptake is much less developed than is that of canopy transpiration, and in some models it is omitted [e.g., Wang and Jarvis, 1990]. In the ABA approach, g_c is an empirical function of ψ_s or θ , so that these variables directly limit transpiration and hence root water uptake. Alternatively, potential root water uptake may sometimes be calculated from normalized values of root mass and θ [Grote *et al.*, 1998] or hydraulic conductance weighted by soil layer, and used to limit canopy transpiration.

[6] In the hydraulic approach to modeling g_c , the most detailed models calculate root water uptake from water potentials and hydraulic resistances along a soil – root – canopy pathway from single [Tuzet *et al.*, 2003; Williams *et al.*, 1996] or multiple [Li *et al.*, 2004; Zhang *et al.*, 2005] soil layers to single [Li *et al.*, 2004; Tuzet *et al.*, 2003; Zhang *et al.*, 2005] or multiple [Williams *et al.*, 1996] canopy layers. In these models, soil hydraulic resistances are strongly nonlinear functions of ψ_s or θ and of root length densities, while root hydraulic resistances are functions of root surface areas and axis lengths [e.g., Grant, 1998]. Modeling these resistances have been found necessary to the simulation of seasonal precipitation effects on mass and energy exchange [Williams *et al.*, 1998].

[7] The second stage in modeling water deficit effects on CO₂ uptake, the effects of g_c on CO₂ fixation, is less developed than is the modeling of water deficit effects on g_c . In some models, transpiration and net primary productivity (NPP) are directly affected by soil and/or atmospheric water status, avoiding the simulation of g_c entirely [e.g., Zhai *et al.*, 2004], so that interactions between soil and atmospheric water deficits on NPP are not simulated. In models in which g_c is calculated from Ball-Woodrow-Berry or related functions, water deficit effects on CO₂ fixation are sometimes assumed to be entirely nonstomatal (i.e.

water deficits act directly on CO₂ fixation). In these models, CO₂ fixation is multiplied by scaling factors derived from ψ_c [Zhang *et al.*, 2005] or θ when calculating g_c . In other models, water deficit effects on CO₂ fixation are assumed to be entirely stomatal [Williams *et al.*, 1996], or both stomatal and nonstomatal [Li *et al.*, 2004], so that CO₂ fixation arises from a solution for intercellular CO₂ concentration (C_i) at which diffusive and biochemical CO₂ fluxes are equal. Although water deficit effects on CO₂ fixation are known to be exerted through both stomatal and nonstomatal processes, there is not yet a consensus about how these processes should be combined in ecosystem models.

[8] Medrano *et al.* [2002] found from a meta-analysis of CO₂ fixation measurements under water stress that many nonstomatal processes, such as electron transport rates, CO₂- and light-saturated carboxylation rates and carboxylation efficiencies, were better correlated with g_c than with plant water status. This correlation between stomatal and nonstomatal effects on CO₂ fixation was found in a wide range of C₃ species, possibly through their joint effects on C_i . This correlation suggests that both effects could be modeled concurrently from related functions of a common indicator of soil or plant water status. If this correlation is robust, as indicated in the meta-analysis of Medrano *et al.* [2002], then such a model should be able accurately to simulate concurrent changes in C_i and in CO₂ and energy exchange by plants during the development and alleviation of soil water deficits.

[9] Recent developments in theory and instrumentation now permit well constrained model tests of C_i and of CO₂ and energy exchange. Farquhar *et al.* [1989] showed that the ratio of C_i to C_a during CO₂ uptake by plants could be calculated from stable isotope compositions ($\delta^{13}\text{C}$) of leaf tissue and the atmosphere. Values of leaf $\delta^{13}\text{C}$ recorded over time would therefore allow estimates of the C_i at which cumulative CO₂ uptake had occurred from the start of plant growth to the time of measurement, assuming $\delta^{13}\text{C}$ of respiration is the same as that of phytomass [Klumpp *et al.*, 2005]. Continuous rates of CO₂ and energy exchange during plant growth can now routinely be measured by eddy covariance (EC). Concurrent measurements of phytomass $\delta^{13}\text{C}$ and of CO₂ and energy exchange during soil drying would therefore provide strongly constrained tests of changes in C_i and CO₂ uptake modeled from stomatal versus nonstomatal effects. These measurements have been taken during several water deficit periods in a semiarid grassland near Lethbridge, Alberta, Canada [Flanagan *et al.*, 2002; Flanagan and Johnson, 2005; Ponton *et al.*, 2006]. In earlier work [Li *et al.*, 2004], we simulated changes in CO₂ and energy exchange during soil drying with the ecosystem model *ecosys* in which CO₂ fixation was modeled from combined stomatal and nonstomatal effects calculated from related functions of ψ_c . We now extend this testing to include changes in CO₂ and energy exchange measured during more recent water deficits, with further constraint provided by changes in C_i calculated from measurements of leaf $\delta^{13}\text{C}$. We contrast the accuracy of this combined model with alternative models based on stomatal or nonstomatal effects alone.

2. Model Development

[10] A detailed description of *ecosys* can be found in earlier publications [e.g., Grant *et al.*, 1999, 2006a]. Algo-

gorithms of particular relevance to the modeling of stomatal and nonstomatal effects on *GPP* and *NEP* are given below, and a list of variables with definitions and units is given in Appendix A.

2.1. Energy Exchange

[11] Energy exchanges between the atmosphere and terrestrial surfaces are resolved in *ecosys* into those between the atmosphere and the leaf and stem surfaces of each population (e.g. species or cohort) within the plant community, and that between the atmosphere and each of the surfaces (soil, plant residue, snow) of the ground beneath [Grant *et al.*, 1999]. Total energy exchange between the atmosphere and terrestrial surfaces is calculated as the sum of exchanges with all plant and ground surfaces. Surface energy exchange is coupled with soil heat and water transfers, including runoff (Manning), infiltration (Green-Ampt), macropore flow (Poiseuille) and micropore flow (Richards).

[12] Canopy energy exchange in *ecosys* is calculated from an hourly two-stage convergence solution for the transfer of water and heat through a multi-layered multi-population soil-root-canopy system (equations (A1)–(A15) in Grant *et al.* [1999]). The first stage of this solution requires convergence to a value of canopy temperature (T_c) for each plant population at which the first-order closure of the canopy energy balance (net radiation, sensible heat flux, latent heat flux and change in heat storage) is achieved. These fluxes are controlled by aerodynamic (r_a) and stomatal (r_c) resistances. Two controlling mechanisms are postulated for r_c :

[13] 1. At the leaf level, a minimum leaf resistance ($r_{l\min}$ in s m^{-1}) is calculated for each leaf surface defined by population i , branch or tiller j , node k , layer l , azimuth m , inclination n , and exposure (sunlit versus shaded) o . This resistance allows a set ratio of intercellular to canopy boundary CO₂ concentration $C_i^l:C_b$ to be maintained at carboxylation rates V_c^l ($\mu\text{mol m}^{-2} \text{s}^{-1}$) [Farquhar *et al.*, 1980] calculated from chloroplast CO₂ concentration (C_c^l in μM , the aqueous counterpart of C_i^l in $\mu\text{mol mol}^{-1}$) under ambient irradiance, T_c , C_a and full turgor ($\psi_c = 0$ MPa):

$$r_{l\min,i,j,k,l,m,n,o} = (C_b - C_i^l) / V_c^l \quad (1)$$

C_b is calculated from C_a , r_a , and the sum of all net CO₂ exchange by canopy, residue and soil surfaces. V_c^l is then used with $C_i^l:C_b$ at full turgor to calculate $r_{l\min}$ (equation (1)) which is then aggregated by leaf surface area to canopy minimum r_c ($r_{c\min}$ in s m^{-1}) for use in the energy balance convergence scheme (equations (A38)–(A47) in Grant *et al.* [1999]). Carboxylation rates at ambient ψ_c and C_i (V_c in $\mu\text{mol m}^{-2} \text{s}^{-1}$) are solved at a later stage in the calculations as described in CO₂ Fixation (equation (5) below).

[14] 2. At leaf and canopy levels, r_l and r_c are then raised from $r_{l\min}$ and $r_{c\min}$ at full turgor through an exponential function of canopy turgor potential ψ_t in MPa:

$$r_{l,i,j,k,l,m,n,o} = r_{l\min,i,j,k,l,m,n,o} + (r_{l\max,i} - r_{l\min,i,j,k,l,m,n,o})e^{(-\beta\psi_t)} \quad (2a)$$

$$r_{c,i} = r_{c\min,i} + (r_{c\max,i} - r_{c\min,i})e^{(-\beta\psi_t)} \quad (2b)$$

The value of β in equation (2a) retains the value of 5 MPa^{-1} used in earlier studies [e.g., Li *et al.*, 2004; Grant *et al.*, 1999, based on Zur and Jones, 1981]. The value of ψ_t is determined from ψ_c and osmotic water potential ψ_π generated during convergence for transpiration versus water uptake (equation (3) under Water Relations below). There is no direct response of r_c to D in *ecosys*, although such a response is included in most other models of r_c . However, larger D raises transpiration, forcing lower ψ_c and ψ_t to be calculated from soil and root hydraulic resistances during convergence for transpiration versus water uptake. The exponential function used to calculate r_c from ψ_t (equation (2)) causes r_c to become more sensitive to ψ_t as ψ_c and ψ_t decline. In wet soil, ψ_t may be high enough that r_c is not very sensitive to diurnal variation in D , as has been found experimentally by Garcia *et al.* [1998]. However, in drying soil with lower ψ_t , r_c becomes more sensitive to D , as found experimentally by Wever *et al.* [2002].

2.2. Water Relations

[15] After convergence for T_c is achieved, the difference between canopy transpiration from the energy balance (from the difference between vapor pressure of the atmosphere e_a and canopy $e_{c_{\text{TEI}}}$ in $\text{m}^3 \text{m}^{-3}$) and total water uptake from all rooted layers in the soil (soil-canopy ψ gradient divided by soil and root hydraulic resistances Ω_s and Ω_r (MPa s m^{-1}) in each rooted soil layer l) is tested against the difference between canopy water content (product of canopy mass M_c and water concentration θ_c) between the current and previous hour (all fluxes in $\text{m}^3 \text{m}^{-2} \text{s}^{-1}$) [Grant *et al.*, 1999]:

$$(e_a - e_{c_{\text{TEI}}}) / (r_{a_i} + r_{c_i}) - \sum_l \sum_z (\psi_{c_i} - \psi_{s_l}) / (\Omega_{s_{l,z}} + \Omega_{r_{l,z}} + \sum_x \Omega_{a_{l,z,x}}) = M_{c(t)} \theta_{c_{\psi_c(t)}} - M_{c(t-1)} \theta_{c_{\psi_c(t-1)}} \quad (3)$$

These differences are minimized by adjusting ψ_c which determines each term in equation (3). For transpiration, ψ_c determines ψ_t , and hence r_c (equation (2)) through its effect on ψ_π (equations (A24) and (A25) in Grant *et al.* [1999]). For root uptake, the difference between ψ_c and ψ_s establishes potential differences across $\Omega_s + \Omega_r$ in each rooted soil layer l (equations (A32)–(A37) in Grant *et al.* [1999]). Values of Ω_s are calculated from radial water flow from soil to root surfaces [Cowan, 1965; Herkelrath *et al.*, 1977]. Values of Ω_r are calculated from a pipe model based on Poiseuille relationships using root radial and axial resistivities [Doussan *et al.*, 1998] with lengths and surface areas of primary and secondary root axes from a root system submodel [Grant, 1998]. Changes in θ_c are determined from those in ψ_c according to M_c and $\psi_c - \theta_c$ relationships. Because r_c and T_c both drive transpiration, the canopy energy balance described under Energy Exchange above is recalculated for each adjusted value of ψ_c during convergence.

2.3. Gross Primary Productivity

[16] After successful convergence for T_c and ψ_c (equation (3)), leaf carboxylation rates V_c under ambient ψ_t (equations (A38)–(A47) in Grant *et al.* [1999]) are reduced from those under full ψ_t (V_c^l in equation (1)) by both stomatal and nonstomatal effects of canopy water status. Stomatal effects are caused by the increase in r_l

from r_{\min} at full ψ_t (equation (2)) to that at ambient ψ_t (from ψ_c in equation (3)). A function for nonstomatal effects on V_c (f_ψ) is derived from the nonlinear relationship with stomatal effects presented by *Medrano et al.* [2002]:

$$f_{\psi_{i,j,k,l,m,n,o}} = (r_{l \min_{i,j,k,l,m,n,o}} / r_{l_{i,j,k,l,m,n,o}})^\chi \quad (4)$$

where $\chi = 0.5$. Equation (4) is not intended to indicate that nonstomatal effects are a function of stomatal effects, but rather that both are functions of canopy water status (in this case ψ_t , which is itself a function of ψ_c , through equation (2)). However, nonstomatal effects in equation (4) are less sensitive to canopy water status than are stomatal effects, as found experimentally by *Ennahli and Earl* [2005]. The value of f_ψ is used to constrain both CO₂-limited and light-limited reaction rates used to calculate V_c under ambient ψ_t (equation (5)). At this stage of model development, this constraint is assumed to be the same for both rates, although some experimental evidence suggests that the light-limited rate may be more affected [*Kellomaki and Wang*, 1996]. Stomatal and nonstomatal effects are combined by calculating V_c from a convergence solution for C_i in $\mu\text{mol mol}^{-1}$ at which the diffusion of gaseous CO₂ in $\mu\text{mol m}^{-2} \text{s}^{-1}$ between C_b and C_i through r_l (equation (5a)) equals the minimum of the carboxylation rates of aqueous CO₂ at ambient C_c (the aqueous counterpart in μM of C_i) and irradiance (from electron transport J in $\mu\text{mol m}^{-2} \text{s}^{-1}$ and carboxylation efficiency Y in $\mu\text{mol } \mu\text{mol}^{-1}$) (equation (5b)), constrained by f_ψ , and by functions of temperature f_{Tc} and nutrient status f_N :

$$\begin{aligned} V_{c_{i,j,k,l,m,n,o}} &= (C_b - C_{i,j,k,l,m,n,o}) / r_{l_{i,j,k,l,m,n,o}} \\ &= \min\{V_{b \max_{i,j,k}}(C_{c_{i,j,k,l,m,n,o}} - \Gamma_{i,j,k}) / (C_{c_{i,j,k,l,m,n,o}}) + K_{c_i}\}, \end{aligned} \quad (5a)$$

$$J_{i,j,k,l,m,n,o} Y_{i,j,k,l,m,n,o} \} f_{\psi_{i,j,k,l,m,n,o}} f_{Tc_i} f_{N_i} \quad (5b)$$

where J is a hyperbolic function of irradiance I in $\mu\text{mol m}^{-2} \text{s}^{-1}$ and quantum yield ε in $\mu\text{mol } \mu\text{mol}^{-1}$, modified by a shape parameter α (0.8):

$$\begin{aligned} J_{i,j,k,l,m,n,o} &= (\varepsilon I_{i,l,m,n,o} + J_{\max_{i,j,k}} - ((\varepsilon I_{i,l,m,n,o} + J_{\max_{i,j,k}})^2 \\ &\quad - 4\alpha \varepsilon I_{i,l,m,n,o} J_{\max_{i,j,k}})^{0.5}) / (2\alpha) \end{aligned} \quad (5c)$$

I is calculated for each leaf surface from the sum of flux densities absorbed by leaves of known optical properties through direct interception from sun and sky, through forward scattering from canopy layers above, and through reflection and backscattering from canopy layers below.

[17] V_c in equation (5) is driven by the products of specific activities ($\mu\text{mol g}^{-1} \text{s}^{-1}$) and areal concentrations (g m^{-2}) of rubisco and chlorophyll ($V_{b \max}$ and J_{\max} in $\mu\text{mol m}^{-2} \text{s}^{-1}$). Specific activities are inhibited by increases in the nonstructural C pool σ_c to which V_c is added [e.g., *Stitt*, 1991]. This pool accumulates when water status or when nonstructural N or P limit the use of σ_c for phytomass biosynthesis, so that V_c is fully coupled to rates of σ_c removal as controlled by plant water and nutrient status.

Areal concentrations are set from leaf structural N and P concentrations which are determined by leaf nonstructural N:C and P:C ratios controlled by CO₂ fixation versus N and P uptake during growth. The calculation of V_c in equation (5) is identical to that of V'_c in equation (1), except that C_i and C_c replace C'_i and C'_c in equation (5a), and f_ψ appears in equation (5b).

[18] The V_c at convergence is added for each leaf surface in the canopy to arrive at a value for gross primary productivity ($GPP = \sum_i \sum_j \sum_k \sum_l \sum_m \sum_n \sum_o V_{c_{i,j,k,l,m,n,o}}$) by each plant population (i.e. species or cohort) in the model.

2.4. Autotrophic Respiration

[19] V_c is added to nonstructural C pools σ_c (g C m^{-2}) in each tiller. These pools exchange nonstructural C with σ_c in each root layer according to concentration gradients of σ_c driven by production V_c in tillers versus respiration R_c in tillers and roots [*Grant*, 1998]. These σ_c pools undergo first-order oxidation ($R'_c = 0.015 \text{ h}^{-1}$ at 25°C) to meet autotrophic respiration requirements in tillers (equation (6a)) and roots (equation (6b)):

$$R_{c_{i,j}} = R'_c \sigma_{c_{i,j}} f_{T_{a_i}} \quad (6a)$$

$$R_{c_{i,l,z}} = R'_c \sigma_{c_{i,l,z}} f_{T_{a_{i,l}}} \quad (6b)$$

R_c is first used to meet requirements for maintenance respiration R_m , a temperature-dependent function ($Q_{10} = 2.25$) of structural N content (specific rate = $0.1125 \text{ g C g N}^{-1} \text{ h}^{-1}$ at 25°C), then any excess is used for growth respiration R_g to drive biosynthesis according to organ-specific growth yields [e.g., *Penning de Vries*, 1982]. Low σ_c may cause R_c to become less than R_m , in which case the shortfall is made up through respiration of remobilizable protein C (R_s in equation (7)) withdrawn from lamina and sheath C at each node proceeding upwards (equation (7a)), or root axis (equation (7b)), until R_m requirements are met:

$$R_{s_{i,j}} = -\min\{0.0, R_{c_{i,j}} - R_{m_{i,j}}\} \quad (7a)$$

$$R_{s_{i,l,z}} = -\min\{0.0, R_{c_{i,l,z}} - R_{m_{i,l,z}}\} \quad (7b)$$

Upon exhaustion of the remobilizable protein C in each lamina, sheath, or root, the remaining structural C is dropped from the plant and added to the soil surface or soil profile as litter. Environmental constraints such as water, heat or nutrient stress (f_ψ , f_{Tc} or f_N in equation (5b)) that reduce V_c , σ_c and hence R_c with respect to R_m will therefore hasten litterfall from the plant. Autotrophic respiration (R_a in equation (8)) is the sum of R_c and R_s in shoots and roots:

$$R_{a_i} = \sum_j (R_{c_{i,j}} + R_{s_{i,j}}) + \sum_l \sum_z (R_{c_{i,l,z}} + R_{s_{i,l,z}}) \quad (8)$$

[20] NPP is calculated as the difference between GPP (from canopy-aggregated V_c in equation (5)) and R_a (equation (8)).

2.5. Heterotrophic Respiration

[21] Soil organic transformations in *ecosys* occur in five organic matter–microbe complexes i (coarse woody litter,

fine nonwoody litter, animal manure, particulate organic matter (*POM*), and humus) in surface residues and in each soil layer l . Each complex consists of five organic states: solid organic matter S , dissolved organic matter DOC , sorbed organic matter, microbial biomass M , and microbial residues, all in g C m^{-2} . Coarse woody and fine nonwoody litterfall are partitioned into components j including carbohydrate, protein, cellulose, and lignin, each of which is of differing vulnerability to hydrolysis by heterotrophic decomposers. These components are further resolved into elemental contents C, N and P. Hydrolysis rates D_s ($\text{g C m}^{-2} \text{h}^{-1}$) in each i are driven by the active biomass M_b of all heterotrophic microbial functional types n (obligately aerobic, facultatively anaerobic (denitrifiers), obligately anaerobic (fermenters and acetotrophic methanogens), and nonsymbiotic diazotrophs) in each organic matter–microbe complex:

$$D_{s_{i,j,l}} = D'_{s_{i,j,l}} \sum_n M_{b_{i,n,l}} f_{Tm_i} \quad (9)$$

Specific hydrolysis rates D'_s ($\text{g S g M}^{-1} \text{h}^{-1}$) are nonlinear functions of a maximum rate D'_s and the concentration of S ($[S] = S/\text{soil mass in g C Mg}^{-1}$) undergoing hydrolysis:

$$D'_{s_{i,j,l}} = \left\{ D'_s [S_{i,j,l}] \right\} / \left\{ [S_{i,j,l}] + K_{m_D} (1.0 + \sum_n [M_{b_{i,n,l}}] / K_{i_D}) \right\} \quad (10)$$

D_s is controlled by soil temperature T_s through an Arrhenius function f_{Tm} in equation (9), and by θ through its effect on aqueous microbial concentrations ($[M_b] = M_b/\theta$ in g C m^{-3}) through an inhibition constant (K_{i_D} in g C m^{-3}) based on kinetics proposed by *Lizama and Suzuki* [1990]. Most $D_{s_{i,j \neq \text{lignin},l}}$ (nonlignin hydrolysis product) is released as DOC used for heterotrophic growth and respiration (equation (11)). $D_{s_{i,j = \text{lignin},l}}$ combines with some $D_{s_{i,j = \text{protein, carbohydrate},l}}$ to form *POM*.

[22] Heterotrophic respiration (R_h in $\text{g C m}^{-2} \text{h}^{-1}$) is conducted by M_b of each n in each i of each l consuming DOC according to Michaelis-Menten kinetics ($K_{m_{DOC}} = 36 \text{ g C m}^{-3}$ [from *McGill et al.*, 1981]) (equation (11)). R_h is driven by maximum specific rate R'_h ($= 0.15 \text{ g g}^{-1} \text{h}^{-1}$ at 25°C) and constrained by DOC concentration ($[DOC] = DOC/\theta$ in g C m^{-3}), and by microbial N and P concentrations C_N and C_P with respect to maximum values C'_N and C'_P .

$$R_{h_{i,n,l}} = M_{b_{i,n,l}} \left\{ R'_h [DOC_{i,l}] \right\} / \left\{ (K_{m_{DOC}} + [DOC_{i,l}]) \right\} \cdot \min \left\{ C_{N_{i,n,j,l}} / C'_{N_j}, C_{P_{i,n,j,l}} / C'_{P_j} \right\} f_{Tm_i} \quad (11)$$

C_N and C_P are determined by the availability of $DON + NH_4^+ + NO_3^-$ versus DOC . CO_2 emission from the soil surface is driven by $R_h = \sum_i \sum_n \sum_l R_{h_{i,n,l}}$ and by belowground R_a (equation (8)) through volatilization and diffusion. Further details about the calculation of R_h may be found in *Grant et al.* [1993a, 1993b]. There are also autotrophic microbial functional types in the model including nitrifiers, methanogens and methanotrophs that take up CO_2 at low rates. Microbial decomposition products are partitioned

between humus and microbial residues according to soil clay content.

[23] NEP is calculated as GPP (equation (5)) $- R_a$ (equation (8)) $- R_h$ (equation (11)). Values for all input parameters in equations (1)–(11) remain unchanged from those used in earlier studies (see Appendix A in *Grant et al.* [2006a]).

3. Field Experiment

3.1. Description of Field Site

[24] The field site was established in June 1998 approximately 1.5 km west of Lethbridge, Alberta, Canada (49.43°N , 112.56°W , 951 masl) on 64 ha of an Orthic Dark-Brown Chernozem (Table 1) under an ungrazed, mixed grass prairie dominated by *Agropyron* spp. with a variety of other species present including *Vicia americana*, *Koleria cristata*, *Eurotia lanata*, *Stipa comata*, *Achillea millefolium*, *Artemisia frigida*, *Carex* spp., *Tragopogon dubius*, and *Bouteloua gracilis*. The long-term mean annual precipitation (1908–1999) was 401 mm, often with a single peak early in the summer followed by moderate to severe water deficits. Average annual potential evapotranspiration is 681 mm, so that the site is classified as semiarid.

3.2. Measurement of Energy and CO₂ Fluxes

[25] Eddy covariance (EC) has been used to measure CO_2 and energy exchange on a continuous basis since June 1998 [*Flanagan and Johnson*, 2005; *Flanagan et al.*, 2002; *Wever et al.*, 2002]. A three-dimensional ultrasonic anemometer (Solent 1012, Gill Instruments Ltd., Lymington, England) was mounted on a one meter boom placed on top of a 6 meter tower and oriented in the prevalent wind direction (west) to measure wind speed, direction and air temperature. Changes in CO_2 and water vapor concentration were measured with a closed path, fast response infrared gas analyzer (IRGA) (LI-6262, LI-COR Inc., Lincoln, Nebraska) housed in an insulated instrument hut. Air for CO_2 and water vapor measurements was drawn at 8 L min^{-1} through 15 m of tubing (3 mm inner diameter Bev-A-Line IV Tubing, LABCOR, Concord, Ontario) by a diaphragm pump (Capex V2X 12 VDC, Charles Austen Pumps Ltd., Surrey, England, or KNF UN828 KNI, KNF Neuberger Inc, Trenton, New Jersey) placed downstream from the IRGA. Fluxes of water vapor, CO_2 , and sensible heat were computed using the University of Edinburgh EdiSol software [*Moncrieff et al.*, 1997]. Protocols for screening and gap-filling CO_2 fluxes are described in *Barr et al.* [2004] and *Flanagan and Johnson* [2005]. Gross CO_2 uptake ($=GPP$) was calculated by adding estimated daytime ecosystem respiration to measured and gap-filled daytime CO_2 fluxes.

3.3. Measurement of Leaf Carbon Isotope Composition ($\delta^{13}\text{C}$)

[26] Six replicate samples of live aboveground phytomass, collected at two-weekly intervals as described earlier, were dried in an oven at 60°C for at least 24 hours, and then frozen in liquid N and ground. A 1–2 mg subsample of ground material was sealed in a tin capsule and loaded into an elemental analyzer for combustion (Carla Erba). The carbon dioxide generated from the combustion was purified

Table 1. Properties of the Orthic Brown Chernozem at Lethbridge, Alberta as Used in *ecosys*^a

Depth of Layers, m	0.01	0.03	0.05	0.11	0.21	0.30	0.40	0.50	0.70	0.90	1.20
ρ_b , Mg m ⁻³	1.24	1.24	1.24	1.24	1.27	1.27	1.32	1.3	1.37	1.4	1.4
θ_{fc} , m ³ m ⁻³	0.32	0.32	0.32	0.32	0.38	0.38	0.32	0.35	0.28	0.27	0.27
θ_{wps} , m ³ m ⁻³	0.17	0.17	0.17	0.17	0.24	0.24	0.19	0.20	0.15	0.13	0.13
K_{sat} , mm h ⁻¹	12.0	12.0	12.0	12.0	2.0	2.0	3.7	3.7	5.4	5.4	5.4
Sand content, g kg ⁻¹	288	288	288	288	274	274	330	260	385	410	410
Silt content, g kg ⁻¹	400	400	400	400	296	296	333	383	365	370	370
pH	7.1	7.1	7.1	7.1	7.3	7.3	7.4	7.4	7.6	7.5	7.5
Organic C, g C kg ⁻¹	61.1	47.2	31.1	19.2	14.4	15.3	3.0	2.1	1.4	0.7	0
Organic N, g N Mg ⁻¹	4800	3800	2600	1600	1100	1200	275	187	125	63	0

^a Soil texture, organic matter content and pH of A (0 to 0.11 m) and B horizons (0.11 to 0.30 m) were measured at the field site, and those of lower layers were extracted from AGRASID (<http://www.agric.gov.ab.ca/agdex/000/agrasid.html>). ρ_b , θ_{fc} , θ_{wps} and K_{sat} were calculated from soil texture [Saxton *et al.*, 1986].

in a gas chromatographic column and passed directly to the inlet of a gas isotope ratio mass spectrometer (Delta Plus, Finnigan Mat, San Jose, CA, USA). The carbon isotope ratios of the samples were expressed as $\delta^{13}\text{C}$ values in ‰:

$$\delta = \left[\frac{R_{\text{sample}}}{R_{\text{std}}} - 1 \right] \quad (12)$$

where R is the molar ratio in ‰ of heavy to light isotope in the sample and in the international standard Pee Dee Belemnite (PDB). The $\delta^{13}\text{C}$ values were used to calculate the time-integrated C_i at which the C in the phytomass samples had been fixed during growth:

$$\delta^{13}C_{\text{leaf}} = \delta^{13}C_a - a - (b - a) \cdot C_i/C_a \quad (13)$$

where $\delta^{13}C_a$ is the $\delta^{13}\text{C}$ value of atmospheric source CO₂ relative to PDB (−8‰), a is the discrimination against diffusion of ¹³CO₂ relative to ¹²CO₂ (4.4‰), and b is the discrimination against ¹³CO₂ during C₃ carboxylation (27‰). C_a in equation (13) was taken to be 370 $\mu\text{mol mol}^{-1}$.

3.4. Other Site Measurements

[27] Along with the *EC* instrumentation, a weather station was established to provide meteorological data at ½-hourly intervals. Net radiation and photosynthetic photon flux density (PPFD, 400–700 nm wave band) were measured by a net radiometer (REBS Q*7.1, Radiation Energy Balance System, Seattle, Washington) and a LI-COR Quantum Sensor (LI-190SA, LI-COR, Lincoln, Nebraska) mounted on a nearby 3 m tower. Relative humidity and air temperature were measured using a shielded thermistor and a capacitance humidity probe (207 Temperature and Relative Humidity Probe, Campbell Scientific Ltd., Edmonton, Alberta) placed 2 meters above the ground. Mean soil heat flux was calculated from two soil heat flux transducers (REBS HFT-3.1, Radiation Energy Balance System, Seattle, Washington), placed about 2 cm below the soil surface. Total precipitation was recorded in 15-minute intervals by a tipping bucket rain gauge (TE525, Texas Electronics, Inc., Dallas, Texas) positioned 1 meter above ground approximately 6 m from the *EC* tower. Because we were not equipped to measure precipitation in the form of snow, precipitation data from the Lethbridge Research Centre

(Agriculture and Agri-food Canada) about 10 km away were used from October 1 to April 30. Precipitation data from the LRS were also used when meteorological data from the site were missing.

[28] Aboveground phytomass, leaf area (LI-3100 Area Meter, LI-COR, Lincoln, Nebraska) and surface litter were measured from six replicate samples collected at approximately 2-week intervals within a 20 cm by 50 cm quadrat placed in randomly selected 1 × 1.5 m subplots located within two larger 20 × 20 m plots, one northeast and the other southeast of the instrument hut. Soil water contents were measured gravimetrically once per week from six replicates (0–10 cm in 2001 and 0–15 cm in 2002 and 2003). In 2001, these measurements were converted to volumetric values, averages of which were compared with depth-weighted θ simulated in the upper four soil layers (Table 1). In 2002 and 2003, these measurements were used to calibrate four soil water reflectometers (0–15 cm) (CS-615, Campbell Scientific, Edmonton, Canada), ½-hourly averages of which were compared with depth-weighted average θ simulated in the upper five soil layers.

4. Model Experiment

4.1. Model Testing

[29] *Ecosys* was initialized with the physical properties of the Orthic Dark-Brown Chernozem (Table 1) and the biological properties of C₃ and C₄ grass functional types [Grant *et al.*, 2001, 2004] seeded at 200 and 5 plants m⁻² respectively during the first year of the model run to approximate the composition of the Lethbridge grassland. The model was then run at $C_a = 370 \mu\text{mol mol}^{-1}$ through twelve cycles of a 14-year weather data sequence recorded at Lethbridge from 1991 to 2004 (= 168 years with average annual precipitation of 395 mm). Differing precipitation during 2001, 2002 and 2003 (216, 585 and 273 mm respectively) allowed model behaviour to be evaluated during different degrees of soil water deficits. Therefore during the 124th, 125th and 126th year of the run, in which weather data from 2001, 2002 and 2003 respectively were used, CO₂ and energy fluxes from the model were compared with those measured by *EC*. The modeled impact of soil water deficits on CO₂ fixation was further corroborated by comparing C_i calculated from seasonal measurements of $\delta^{13}\text{C}$ values in aboveground phytomass (equation (13)) with the average C_i at which cumulative CO₂ fixation occurred in

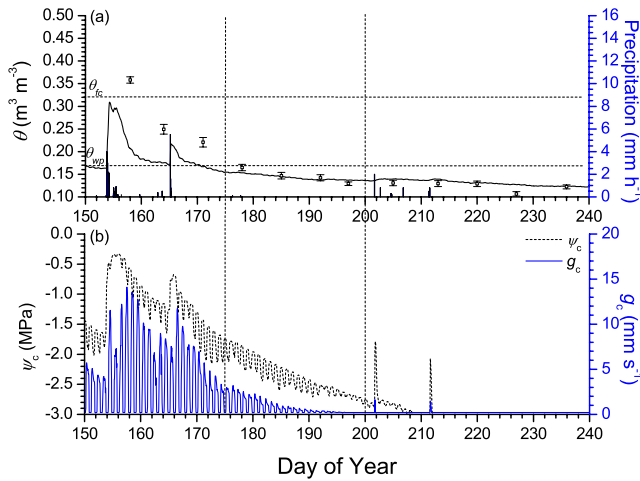


Figure 1. (a) Soil water content (θ), (b) canopy water potential (ψ_c) and stomatal conductance (g_c) modeled (lines) and measured (symbols – average \pm SE of 6 replicates) in a mixed grassland at Lethbridge during 2001. Vertical dashed lines indicate flux comparison period shown in Figure 2.

the model up to any day d during a growing season ($C_{i,d}$), calculated as:

$$C_{i,d} = \frac{\sum_d \sum_i \sum_j \sum_k \sum_l \sum_m \sum_n \sum_o (V_{C_{i,j,k,l,m,n,o}} C_{i,j,k,l,m,n,o})}{\sum_d \sum_i \sum_j \sum_k \sum_l \sum_m \sum_n \sum_o V_{C_{i,j,k,l,m,n,o}}} \quad (14)$$

4.2. Sensitivity to Model Parameterization of Water Deficit Effects on CO₂ Fixation

[30] Earlier work with *ecosys* has shown only a limited sensitivity of stomatal effects on CO₂ uptake to the value of β in equation (2), because larger (smaller) β caused lower (higher) r_c , hence lower (higher) ψ_c (equation (3)), ψ_b and higher (lower) r_c (equation (2)), thereby offsetting the direct effect of β on r_c . Thus variation of $\pm 20\%$ in β caused variation of only $\pm 2\%$ in annual net CO₂ exchange [Li *et al.*, 2004]. We have retained the value of this parameter used in earlier studies of water deficit effects on CO₂ fixation [e.g., Li *et al.*, 2004; Grant *et al.*, 2004, 2006b] because it appeared to give a stomatal sensitivity to plant water status that was consistent with results of more detailed experiments [e.g., Zur and Jones, 1981].

[31] The sensitivity of nonstomatal effects to the parameterization of equation (4) was tested by changing χ from 0.5 to 1 (nonstomatal effects and stomatal effects limit CO₂ fixation equally) or 0 (eliminating nonstomatal effects entirely as found experimentally by Mederski *et al.* [1975]). The first alternative parameterization created a model comparable to ones in which nonstomatal effects on CO₂ fixation are first solved from soil or plant water status, and then CO₂ fixation is used to calculate g_c [e.g., Zhang *et al.*, 2005]. The second alternative parameterization created a model comparable to ones in which CO₂ fixation is calculated from stomatal effects alone [e.g., Williams *et al.*, 1996]. The 124th, 125th and 126th years of the model run under 2001, 2002 and 2003 weather were re-executed with both these alternatives, and results for CO₂ fluxes

(equation (5)) and $C_{i,d}$ (equation (14)) were compared with measured values during soil drying.

5. Results and Discussion

5.1. Hourly CO₂ and Energy Exchange During Soil Drying

[32] Low precipitation during 2001 (216 mm), following low precipitation during 2000 (276 mm), caused θ (0–10 cm) to remain low during spring, and to decline below wilting point (θ_{wp} in Table 1) by late June (Figure 1a). Declines in θ forced declines in ψ_s , rises in Ω_s and Ω_a , and hence rapid declines in ψ_c (equation (3)) and g_c ($= r_c^{-1}$) (equation (2)) (Figure 1b). Lower g_c reduced LE versus H (Figure 2a), indicating strong stomatal limitations to transpiration (equation (3)), especially in July when $\theta < \theta_{wp}$. The strongly nonlinear responses of g_c (equation (2)) and f_ψ (equation (4)) to declining ψ_c forced V_c (GPP with stomatal and nonstomatal effects in equation (5)) to decline from V'_c (GPP without water deficit effects in equation (1)), as water deficits continued (Figure 2b). These declines in V_c were consistent with those in gross CO₂ uptake calculated from EC fluxes. Declining V_c caused modeled CO₂ influxes to remain small and midday declines in modeled CO₂ influxes to begin earlier each day that water deficits continued

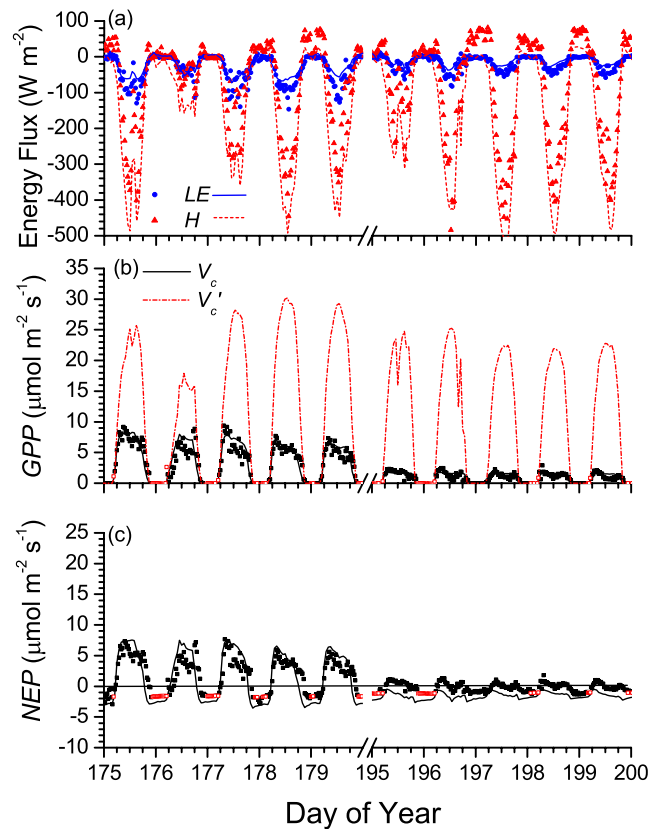


Figure 2. (a) Energy fluxes, (b) gross primary productivity (GPP) with (V_c) and without (V'_c) stomatal and nonstomatal effects, and (c) net ecosystem productivity (NEP) modeled (lines), measured (solid symbols), or gap-filled (open symbols) over a mixed grassland at Lethbridge during June and July 2001. Downward fluxes are positive, upward fluxes are negative.

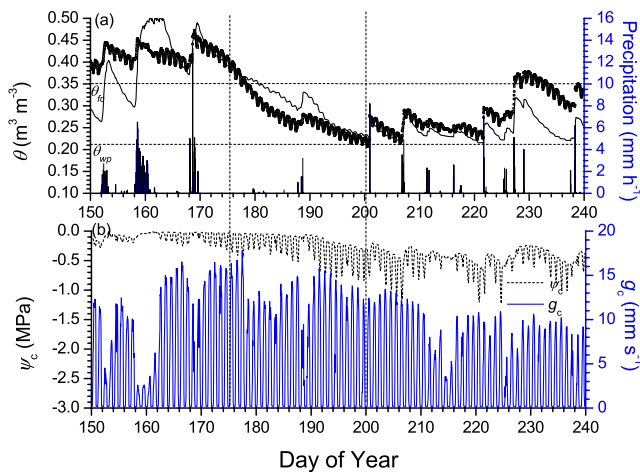


Figure 3. (a) Soil water content (θ), (b) canopy water potential (ψ_c) and stomatal conductance (g_c) modeled (lines) and measured (symbols – average of 4 replicates) in a mixed grassland at Lethbridge during 2002. Vertical dashed lines indicate flux comparison period shown in Figure 4.

(Figure 2c). Declining CO₂ influxes reduced σ_c and hence R_a (equations (6)–(8)), while declining θ raised $[M_{b,i,n}]$ and thereby slowed D_s (equations (9) and (10)) and R_h (equation (11)), so that CO₂ effluxes also declined as water deficits continued (Figure 2c). However, declines in CO₂ influxes were greater than those in effluxes, so that NEP also declined as water deficits continued. The grassland became a net source of CO₂ after DOY 190.

[33] More frequent precipitation during 2002 (585 mm) maintained θ (0–15 cm) above θ_{wp} during the entire growing season (Figure 3a), allowing high ψ_c and g_c (Figure 3b), except during rainy periods (e.g. DOY 151–152, 161–162 or 171–172) when low radiation caused CO₂ fixation and hence g_c to decline (low V'_c in equation (1)). High ψ_c and g_c enabled LE to exceed H (Figure 4a), indicating limited stomatal effects on transpiration (equation (3)). Consequently V_c remained close to V'_c (Figure 4b), as suggested by the consistently rapid gross CO₂ uptake calculated from EC measurements, and CO₂ influxes remained high (Figure 4c), exceeding effluxes during the entire growing season. Maximum CO₂ effluxes in the model were larger than gap-filled EC values (Figure 4c), but were similar to ones of $9 \mu\text{mol m}^{-2} \text{s}^{-1}$ recorded from surface chambers in 2002 by Flanagan and Johnson [2005].

[34] Precipitation during spring 2003, following high precipitation during 2002, maintained θ (0–15 cm) above θ_{wp} until early July, but low precipitation thereafter caused θ to decline below θ_{wp} (Figure 5a), forcing concurrent declines in ψ_c and g_c (Figure 5b). These declines forced LE to decline below H (Figure 6a), indicating a growing stomatal limitation to transpiration (equation (3)) that, combined with a growing nonstomatal limitation (equation (4)), forced V_c to decline from V'_c (Figure 6b). This decline was corroborated by declining gross CO₂ uptake calculated from the EC measurements, and caused CO₂ influxes to decline with respect to CO₂ effluxes (Figure 6c) as water deficits continued from late June through mid-July.

[35] Early soil drying during 2001 (Figure 1a), following low precipitation in 2000, caused phytomass $\delta^{13}\text{C}$ to rise, while high θ during 2002 (Figure 3a) caused phytomass $\delta^{13}\text{C}$ to remain low (Figure 7a). Later soil drying in 2003 (Figure 5a) following high precipitation in 2002 caused only a slight rise in phytomass $\delta^{13}\text{C}$. Consequently C_i calculated from $\delta^{13}\text{C}$ (equation (13)) declined during 2001 and to a lesser extent during 2003, but remained high during 2002 (Figure 7b). In the model, soil drying forced lower ψ_c and g_c during 2001 and to a lesser extent during 2003 (Figures 1b and 5b), causing C_i (equation (14)) to be solved at progressively lower values (Figure 7b). These lower values resulted from the combined effects of rising r_l (equation (2)) and declining f_{ψ} (equation (4)) on V_c and C_i (equation (5)). Higher ψ_c and g_c modeled during 2002 (Figure 3b) allowed C_i to remain near C'_i because r_l remained near r_{lmin} (equation (2)) and f_{ψ} remained near 1.0 (equation (4)), so that V_c and C_i approached V'_c and C'_i (equation (5)). Temporal trends in modeled C_i were consistent with those in C_i calculated from $\delta^{13}\text{C}$ values (Figure 7b).

5.2. Hourly CO₂ and Energy Exchange: Modeled Versus Measured

[36] Agreement between modeled and measured R_n is given in Table 2a. Agreement between modeled and mea-

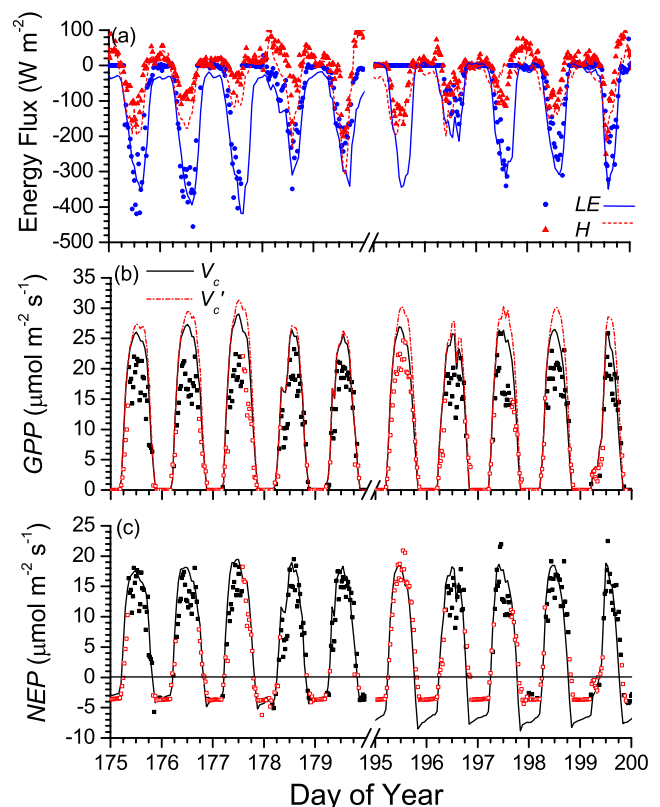


Figure 4. (a) Energy fluxes, (b) gross primary productivity (GPP) with (V_c) and without (V'_c) stomatal and nonstomatal effects, and (c) net ecosystem productivity (NEP) modeled (lines), measured (solid symbols), or gap-filled (open symbols) over a mixed grassland at Lethbridge during June and July 2002. Downward fluxes are positive, upward fluxes are negative.

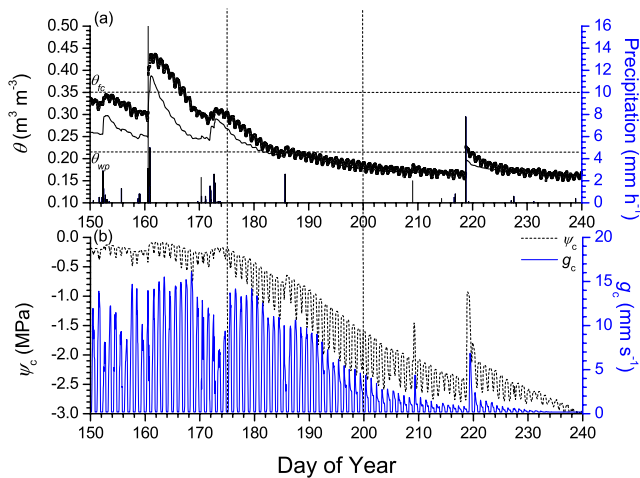


Figure 5. (a) Soil water content (θ), (b) canopy water potential (ψ_c) and stomatal conductance (g_c) modeled (lines) and measured (symbols – average of 4 replicates) in a mixed grassland at Lethbridge during 2003. Vertical dashed lines indicate flux comparison period shown in Figure 6.

sured LE and H during three full years with differing precipitation at Lethbridge ($R^2 = 0.7$ – 0.8 in Tables 2b and 2c) was comparable to that achieved during 1–3 week intervals over grasslands elsewhere [e.g., *Falge et al.*, 2005]. Differences between modeled and measured LE (RSMD ca. 20 W m^{-2}) and H (RSMD ca. 40 W m^{-2}) were about three times the random error in LE and H of 6 and 18 W m^{-2} respectively estimated by *Richardson et al.* [2006] for the grassland at Lethbridge, but were comparable to standard differences in LE and H of 38 and 21 W m^{-2} respectively among different EC systems measured by *Twine et al.* [2000] over grassland. These comparable differences indicate that there may be only limited opportunity to improve agreement between modeled and measured fluxes from that in Tables 2b and 2c.

[37] During years with lower precipitation (2001 and 2003), LE tended to be smaller with respect to H in the model than in the EC measurements ($b_{LE} < b_H$ in Table 2b versus Table 2c; also see Figures 2a and 6a). A lower LE attributed in the model to lower transpiration rather than evaporation could indicate a possible overestimation of r_c (equation (2b)) arising from an overestimation of any of the Ω terms in equation (3). However, transpiration and evaporation cannot be resolved in the measured LE . At an annual time scale, total LE in the model was constrained by annual inputs for precipitation during the two drier years because very little water was lost in runoff or drainage, or left in the soil profile. When precipitation was higher in 2002, LE versus H in the model was consistent with that from EC ($b_{LE} \approx b_H \approx 1.1$ in Tables 2b and 2c).

[38] Agreement between modeled and measured CO₂ exchange at Lethbridge ($R^2 = 0.7$ – 0.8 in Table 2d) indicated that ca. 20% of variance in CO₂ fluxes measured by EC was not explained by the model (Table 2d). The lower correlation found for 2001 was attributed to the small diurnal variation in CO₂ fluxes measured and modeled after early soil drying. Differences between modeled and

measured CO₂ fluxes (RSMD ca. 1 (2001) or 2.5 (2002 and 2003) $\mu\text{mol m}^{-2} \text{ s}^{-1}$) were two to four times the random error in CO₂ fluxes of 0.4 (2001) and 0.6 (2002 and 2003) $\mu\text{mol m}^{-2} \text{ s}^{-1}$ estimated by *Richardson et al.* [2006] for the grassland at Lethbridge. *Twine et al.* [2000] estimated that uncertainty in CO₂ flux measurements by EC over grassland varied between 10% and 30% during a growing season. There may therefore be some opportunity to improve agreement between modeled and measured fluxes in this study.

[39] Under very low precipitation in 2001, CO₂ fluxes tended to be larger relative to LE in the model than in the EC measurements ($b_{CO_2} > b_{LE}$ in Table 2d versus Table 2b). This indicated that C_i in the model may have declined more than in the field during soil drying, although C_i in the model compared well with that derived from $\delta^{13}\text{C}$ values (Figure 7b). Under higher precipitation in 2002 and 2003, the relationship between CO₂ and LE in the model was more consistent with that from EC ($b_{CO_2} \approx b_{LE} \approx 0.9$), corroborating modeled versus measured C_i (Figure 7b).

[40] Agreement between modeled and measured CO₂ fluxes was affected by negative intercepts (a in Table 2d) from regressions of modeled on measured values. These negative a were caused by larger CO₂ effluxes modeled (equations (8) and (11)) versus measured or gap-filled

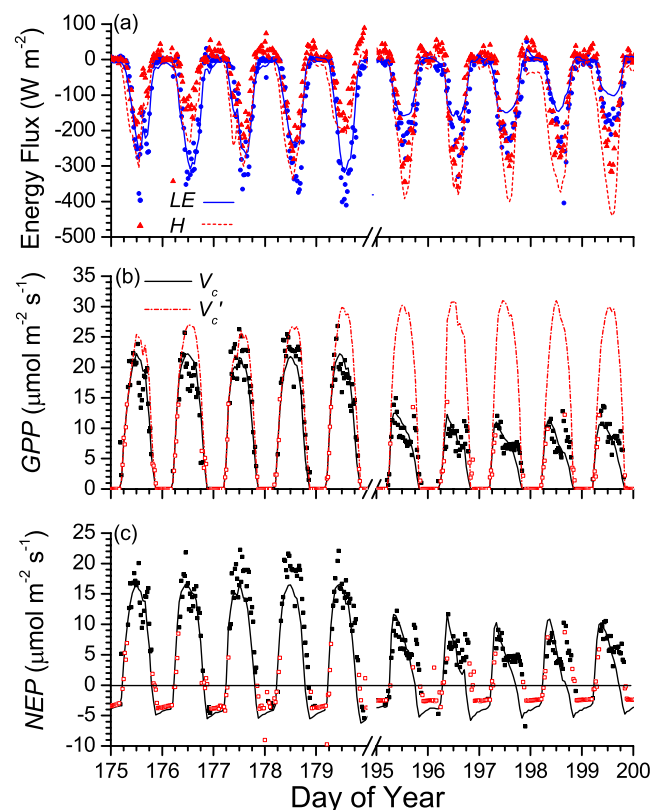


Figure 6. (a) Energy fluxes, (b) gross primary productivity (GPP) with (V_c) and without (V_c') stomatal and nonstomatal effects, and (c) net ecosystem productivity (NEP) modeled (lines), measured (solid symbols), or gap-filled (open symbols) over a mixed grassland at Lethbridge during June and July 2003. Downward fluxes are positive, upward fluxes are negative.

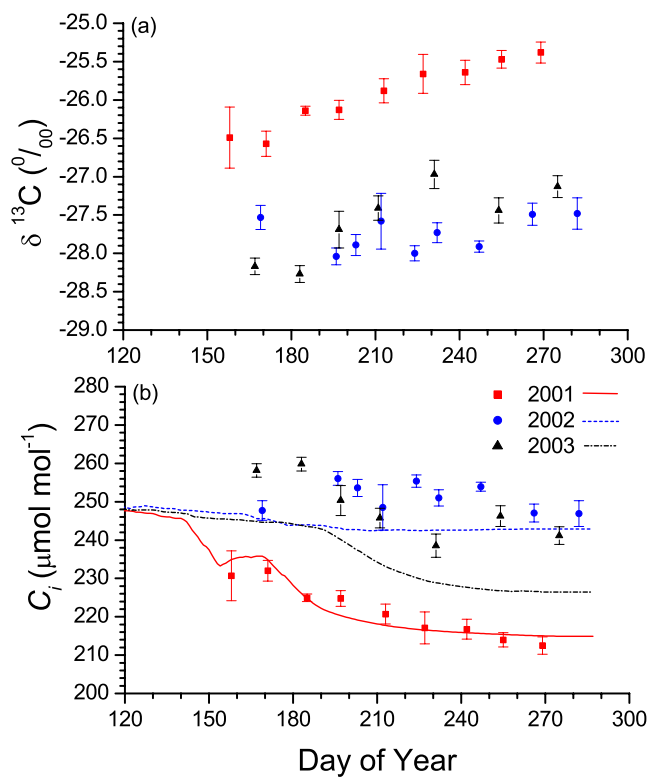


Figure 7. (a) $\delta^{13}\text{C}$ values \pm SE ($n = 6$) in aboveground phytomass, and (b) C_i calculated from $\delta^{13}\text{C}$ values (symbols) versus weighted average C_i of cumulative modeled CO₂ fixation by C₃ grass (lines) in a mixed grassland at Lethbridge during 2001, 2002 and 2003.

during July and early August in all three years of this study. However, CO₂ effluxes modeled before or after this period were in closer agreement with measured or gap-filled values in all three years (e.g. DOY 175–180 versus DOY 195–200 in 2002 in Figure 4c).

5.3. Stomatal Versus Nonstomatal Effects on CO₂ Fixation During Soil Drying

[41] The simulation of water deficit effects on CO₂ exchange in this study depended on modeling both stomatal (equation (2)) and nonstomatal (equation (4)) effects on CO₂ fixation (equations (5a) and (5b), respectively). Stomatal effects were tested against EC measurements of changing

Table 2a. Intercept a , Slope b , Correlation Coefficient R^2 and Root Mean Square for Difference RMSD From the Regressions of Hourly Net Radiation (R_n) From Eddy Covariance Measurements on Fluxes Modeled During 2001, 2002 and 2003

R_n	2001	2002	2003
A_i^a W m ⁻²	1	7	9
B^a	1.08	1.10	1.03
R^2	0.86	0.91	0.89
RMSD, ^b W m ⁻²	58	46	55
N	8758	8615	8442

^a Intercepts and slopes from $y = a + bx$, where y = modeled hourly flux and x = measured hourly-averaged flux (excluding gap-filled values).

^b Root mean square for differences from $y = a + bx$, where y = measured hourly-averaged flux (excluding gap-filled values) and x = modeled hourly flux.

Table 2b. Intercept a , Slope b , Correlation Coefficient R^2 and Root Mean Square for Difference RMSD From the Regressions of Hourly Latent Heat (LE) From Eddy Covariance Measurements on Fluxes Modeled During 2001, 2002 and 2003

LE	2001	2002	2003
A_i^a W m ⁻²	-5	-16	-7
B^a	0.81	1.15	0.75
R^2	0.72	0.84	0.81
RMSD, ^b W m ⁻²	18	21	25
N	8287	7999	7736

^a Intercepts and slopes from $y = a + bx$, where y = modeled hourly flux and x = measured hourly-averaged flux (excluding gap-filled values).

^b Root mean square for differences from $y = a + bx$, where y = measured hourly-averaged flux (excluding gap-filled values) and x = modeled hourly flux.

LE versus H during soil drying (Figures 2a, 4a, and 6a). Nonstomatal effects were tested against CO₂ uptake during stomatal limitation (Figures 2b, 4b, and 6b), and against the C_i at which this uptake occurred (Figure 7b). The alternative parameterizations of nonstomatal effects in equation (4) (changing χ from 0.5 to 1 or 0) did not directly affect r_c in equation (3) so that energy exchange modeled with each alternative remained indistinguishable from that in Figures 2a, 4a, and 6a. However, when nonstomatal effects were set equal to stomatal effects ($\chi = 1$), CO₂ uptake in the model declined more rapidly during soil drying than was measured by EC in both 2001 (Figure 8a) and 2003 (Figure 8c). Conversely when nonstomatal effects were eliminated ($\chi = 0$), CO₂ uptake in the model declined more slowly. These alternative parameterizations had little effect on CO₂ fluxes modeled under higher precipitation in 2002 (Figure 8b).

[42] The alternative parameterizations of nonstomatal effects altered CO₂ uptake through their effects on C_i . When nonstomatal effects were set equal to stomatal effects, the C_i at which CO₂ uptake occurred in the model did not decline during soil drying in 2001 (Figure 9a) and 2003 (Figure 9c) although declines in C_i were apparent in the $\delta^{13}\text{C}$ values. Modeled C_i did not decline with this parameterization because gaseous CO₂ diffusion (equation (5a)) and biochemical CO₂ fixation (equation (5b)) were constrained equally by water deficits, so that C_i and C_c were always solved at values that approached C_i' and C_c' . However, when nonstomatal effects were eliminated, C_i in the model was solved at values that declined more rapidly than did those indicated by $\delta^{13}\text{C}$ values during soil drying in 2001 (Figure 9a) and 2003 (Figure 9c). The rapid decline in C_i

Table 2c. Intercept a , Slope b , Correlation Coefficient R^2 and Root Mean Square for Difference RMSD From the Regressions of Hourly Sensible Heat (H) From Eddy Covariance Measurements on Fluxes Modeled During 2001, 2002 and 2003

H	2001	2002	2003
A_i^a W m ⁻²	-21	-23	-29
B^a	1.08	1.11	1.10
R^2	0.81	0.72	0.79
RMSD, ^b W m ⁻²	44	37	39
N	8329	8099	7758

^a Intercepts and slopes from $y = a + bx$, where y = modeled hourly flux and x = measured hourly-averaged flux (excluding gap-filled values).

^b Root mean square for differences from $y = a + bx$, where y = measured hourly-averaged flux (excluding gap-filled values) and x = modeled hourly flux.

Table 2d. Intercept a , Slope b , Correlation Coefficient R^2 and Root Mean Square for Difference RMSD From the Regressions of Hourly CO₂ Fluxes From Eddy Covariance Measurements on Fluxes Modeled During 2001, 2002 and 2003

CO ₂	2001	2002	2003
A_i^a , $\mu\text{mol m}^{-2} \text{s}^{-1}$	-0.3	-0.4	-0.8
B^a	1.28	0.92	0.81
R^2	0.73	0.80	0.82
RMSD, b , $\mu\text{mol m}^{-2} \text{s}^{-1}$	0.9	2.6	2.4
N	5898	2963	2557

^a Intercepts and slopes from $y = a + bx$, where y = modeled hourly flux and x = measured hourly-averaged flux (excluding gap-filled values).

^b Root mean square for differences from $y = a + bx$, where y = measured hourly-averaged flux (excluding gap-filled values) and x = modeled hourly flux.

with this parameterization occurred when gaseous CO₂ diffusion (equation (5a)) was constrained by water deficits but biochemical CO₂ fixation was not (equation (5b)), forcing C_i and C_c to be solved at values much lower than C_i' and C_c' . These alternative parameterizations had little effect on C_i modeled under higher precipitation in 2002 when declines in C_i were neither modeled nor measured (Figure 9b). No declines in C_i were modeled in 2002 because in the absence of water deficit constraints on diffusion and fixation, C_i and C_c were solved at values that approached C_i' and C_c' .

[43] As soil drying progressed during 2001 and 2003, CO₂ fixation modeled with alternative parameterizations of nonstomatal effects diverged more strongly, and their comparative accuracy could be more clearly distinguished (Figure 9). This divergence indicated that models in which stomatal and nonstomatal effects are assumed equal ($\chi = 1$) could overestimate declines in CO₂ fluxes with respect to those in LE during water deficits [e.g., Ferreyra *et al.*, 2003]. Such overestimates are apparent in these models when $b_{\text{CO}_2} < b_{LE}$ in regressions of modeled on measured fluxes during water deficits [e.g., Zhang *et al.*, 2005]. Conversely, models in which nonstomatal effects are absent ($\chi = 0$) could underestimate declines in CO₂ fluxes with respect to those in LE during water deficits [e.g., Williams *et al.*, 1998]. These findings indicate the need to represent both stomatal and nonstomatal effects when modeling CO₂ fixation, especially during severe water deficits. Declining C_i calculated from $\delta^{13}\text{C}$ values during soil drying indicated that nonstomatal effects were less sensitive to plant water status than were stomatal effects. Therefore nonstomatal effects could be represented by a parameterization such as that in equation (4) ($0 < \chi < 1$) based on the meta-analyses of Medrano *et al.* [2002].

5.4. Annual Primary Productivity

[44] The accurate parameterization of nonstomatal effects on CO₂ fixation was necessary to the simulation of water deficit effects on annual GPP . Low residual soil water from 2000 plus low rainfall during 2001 caused GPP modeled and derived from gap-filled EC measurements to be severely limited by soil water deficits (Figure 1a). These deficits lowered plant water status (Figure 1b), LE versus H (Figure 2a), and hence gross and net CO₂ uptake (Figures 2b and 2c), so that the grassland became a net C source after the end of June. Cool spring temperatures during 2002

delayed leafout and lowered early season GPP . Frequent rainfall thereafter (Figure 3a) maintained plant water status (Figure 3b), LE versus H (Figure 4a), and hence CO₂ uptake (Figure 4b), raising GPP so that the modeled and measured grassland remained a large net C sink until September. Residual soil water from 2002 plus spring rainfall in 2003 delayed the onset of soil water deficits (Figure 5a) and hence the decline of plant water status (Figure 5b), LE versus H (Figure 6a), and CO₂ uptake (Figure 6b). These delays allowed rapid early-season GPP that enabled the grassland to remain a net C sink until late July.

[45] Daily totals of GPP from modeled versus gap-filled EC CO₂ fluxes (e.g. Figures 2b, 4b, and 6b) reached higher values in early summer with greater spring precipitation in 2002 and 2003 versus 2001, and declined earlier with summer drought in 2001 and 2003 versus 2002 (Figure 10). GPP modeled during June and July was frequently larger than gap-filled GPP because modeled CO₂ effluxes were frequently larger than gap-filled EC effluxes while modeled CO₂ influxes were similar to EC CO₂ influxes (e.g. Figure 4c). Annual modeled versus gap-filled GPP rose with precipitation from 397 versus 280 g C m⁻² in 2001, to 844 versus 816 g C m⁻² in 2002 and 636 versus 685 g C m⁻² in 2003. These rises in GPP drove rises in NPP , thereby increasing

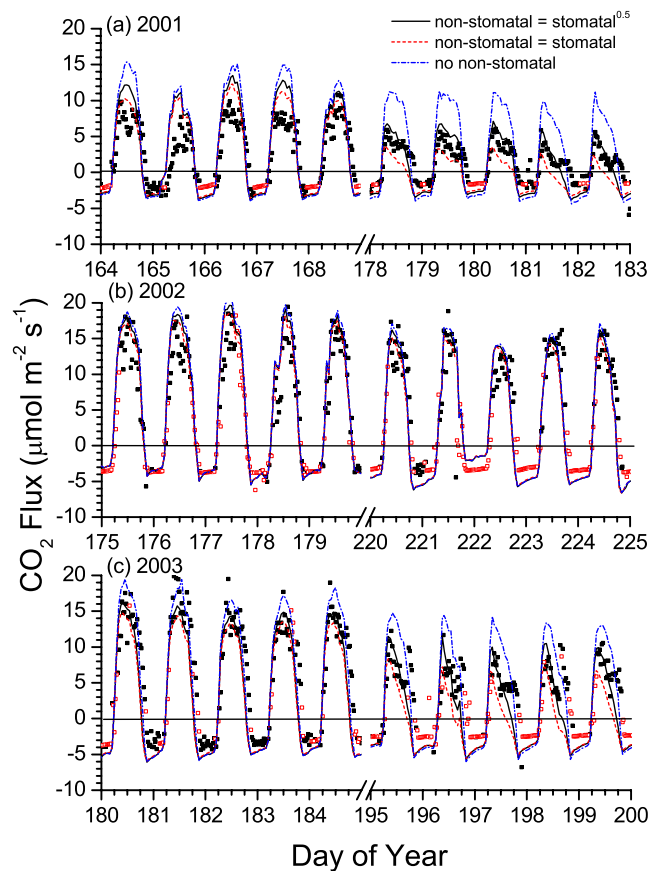


Figure 8. Net ecosystem productivity (NEP) modeled (lines), measured (solid symbols), or gap-filled (open symbols for CO₂) over a mixed grassland at Lethbridge during 2001, 2002 and 2003 for three alternative parameterizations of nonstomatal effects on CO₂ fixation (equation (4) in text).

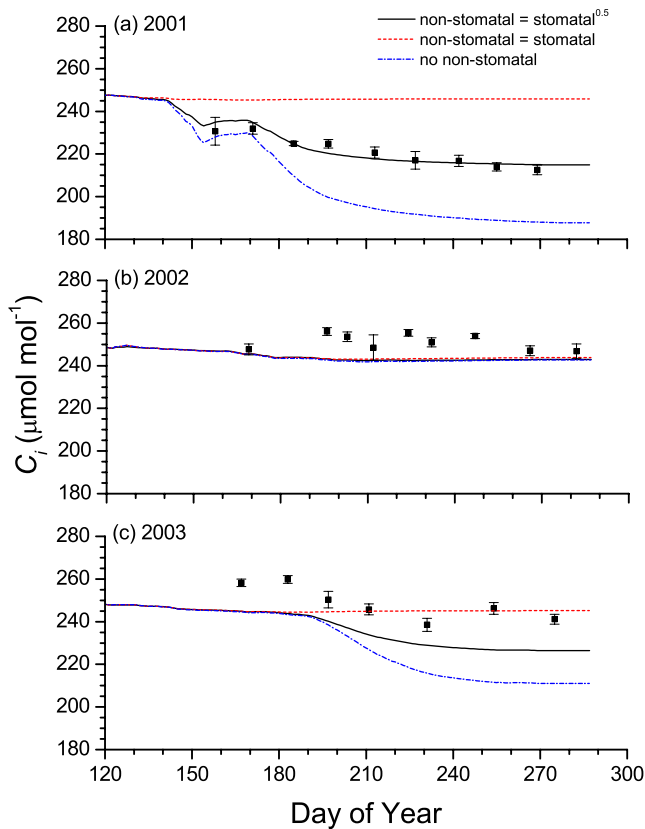


Figure 9. C_i calculated from $\delta^{13}\text{C}$ values in aboveground phytomass (symbols) versus weighted average C_i of cumulative modeled CO₂ fixation (lines) by C₃ grass in a mixed grassland at Lethbridge during 2001, 2002 and 2003 for three alternative parameterizations of nonstomatal effects on CO₂ fixation (equation (4) in text).

LAI (Figure 11a) and shoot mass (Figure 11b), although shoot mass modeled during the wettest year 2002 was greater than that measured. Much of the GPP in the model was invested below ground so that root NPP was 0.7 of total NPP while root mass was 2–3 times larger than shoot mass, except under high precipitation in 2002 (Figure 11c). These results were consistent with root:total NPP ratios for temperate dry grasslands in the meta-analysis of Hui and Jackson [2006], and indicated the large contribution of roots to C transformation and exchange in grassland ecosystems. This contribution was important to modeling the rise in r_l and the decline in V_c during soil drying in 2001 and 2003 (Figures 1 and 5), because r_l was determined by Ω_s and Ω_r (equation (3)) modeled from root density through the soil profile. Values of Ω_s and Ω_r were reduced in the deeper soil during drying of the upper soil by increasing the allocation of C in the model to root versus shoot growth (2001 and 2003 versus 2002 in Figures 11b and 11c), and to deeper versus shallower root growth (2001 and 2003 versus 2002 in Figures 12a–12d) through equation (6b). This allocation hastened water uptake from the deeper soil to sustain LE during soil drying.

5.5. Centennial Ecosystem Productivity

[46] The modeled effects of soil water deficit on CO₂ fixation determined the modeled effects of precipitation on

long-term ecosystem productivity. Precipitation rates varied from 216 to 639 mm y⁻¹ during the 14-year hourly weather record (1991–2004) currently available from the Lethbridge site (Figure 13a), causing NEP in the model ($= \sum_{d=1,365} \sum_{h=1,24} [GPP \text{ (equation (5))} - R_a \text{ (equation (8))} - R_h \text{ (equation (11))}]$) to vary from minimum values of -100 g C m⁻² y⁻¹ (net C source) during drier years to maximum values of +150 g C m⁻² y⁻¹ (net C sink) during wetter years (Figure 13b). Interannual variation in modeled NEP was more closely correlated with that in GPP ($R^2 = 0.74$) than that in R_e ($R^2 = 0.42$), indicating the importance of accurately simulating water deficit effects on CO₂ fixation when simulating NEP.

[47] Changes in modeled NEP from negative values during drier years to positive values during wetter years were consistent with findings from other EC studies of grasslands under variable precipitation at Lethbridge [Flanagan et al., 2002] and elsewhere [Meyers, 2001; Novick et al., 2004; Suyker et al., 2003]. In these studies, changes in NEP with precipitation were attributed mostly to changes in GPP rather than R_e , as modeled here. The regression of annual NEP on precipitation from the model run indicated that this grassland required a precipitation rate of 352 mm y⁻¹ (ca. 0.5 of ET_p) to maintain current SOC ($NEP = 0$). Each mm y⁻¹ of precipitation above or below this rate would cause a gain or loss of 0.49 g C m⁻² y⁻¹. However, this regression explained only 50% of variation in modeled annual NEP because some of

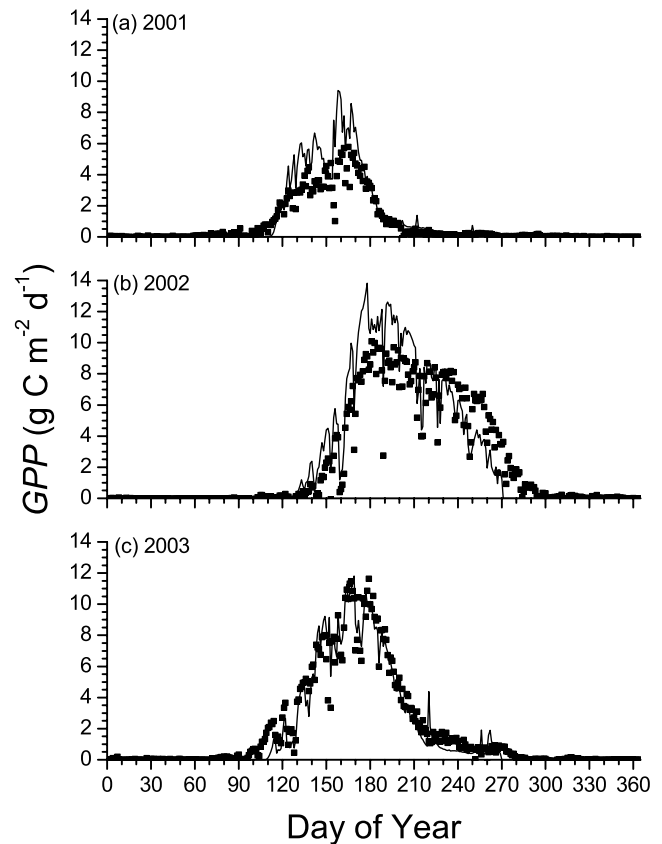


Figure 10. Gross primary productivity (GPP) modeled (lines) or derived from gap-filled eddy covariance measurements (symbols) over a mixed grassland at Lethbridge during 2001, 2002 and 2003.

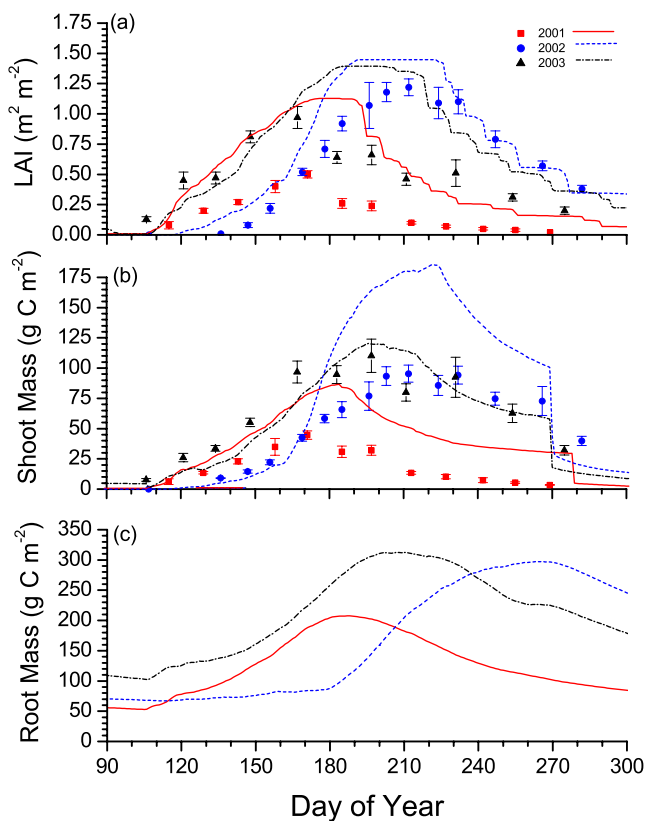


Figure 11. (a) Leaf area index (*LAI*), (b) shoot mass and (c) root mass measured (symbols) and modeled (lines) in a mixed grassland at Lethbridge during 2001, 2002 and 2003.

this variation was attributed to stocks of soil water and plant litterfall carried over from the previous year (e.g. a larger than expected *NEP* modeled in 2003 followed higher than average precipitation in 2002), or to seasonality of precipitation during the current year.

[48] For the precipitation rates over the period of record, modeled *NEP* drove gains in *SOC* (0–1.2 m) that declined

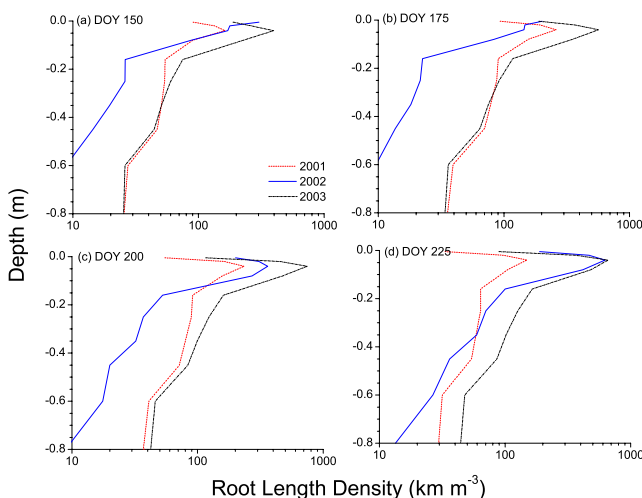


Figure 12. Vertical distribution of root length density modeled in a mixed grassland at Lethbridge on 4 days during the growing seasons of 2001, 2002 and 2003.

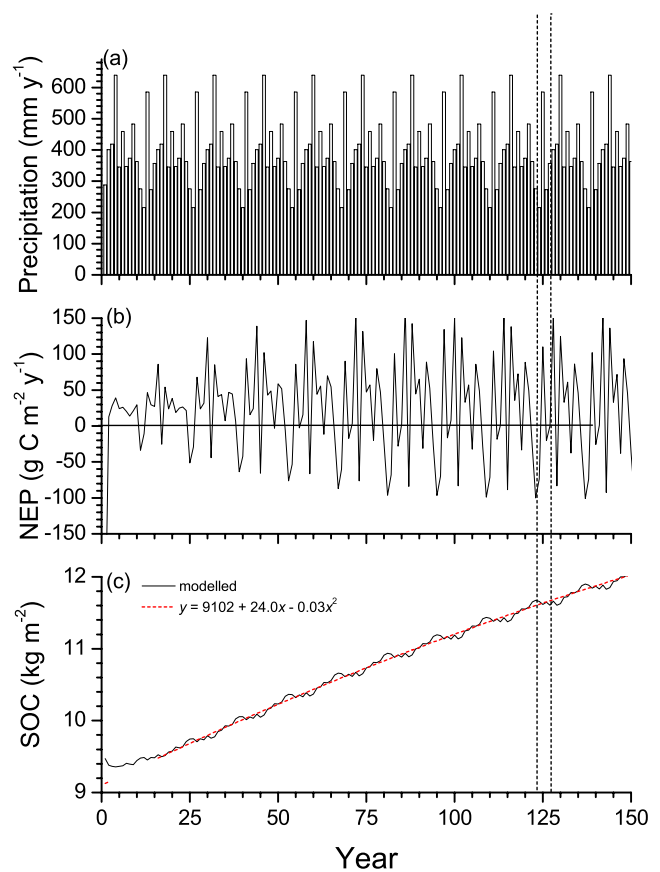


Figure 13. (a) Annual precipitation, (b) annual net ecosystem productivity (*NEP*), and (c) soil organic C (*SOC* = humus + litter) modeled under repeating 14-year sequences of weather data recorded from 1991 to 2004 over a mixed grassland at Lethbridge. Vertical dashed lines indicate period representing 2001–2003 from which modeled data were taken for this study.

from 24 to 15 g C m⁻² y⁻¹, although with considerable interannual variation, during the 150 years of the model run (Figure 13c). These gains did not account for any losses of C from disturbance, such as grazing or fire, and so do not represent net biome productivity (*NBP*) of this ecosystem. Nonetheless, these gains were consistent with one of 28 ± 4 g C m⁻² y⁻¹ (0–1.2 m) reported by *Anderson* [1977] for a cool dry grassland in southern Saskatchewan, and with ones of 7–34 g C m⁻² y⁻¹ (0–0.07 m) found by *White et al.* [1976] for different grass pastures in South Dakota. The grasslands in these studies were aggrading after disturbance, so that these measured *SOC* gains may have been larger than those that would have been measured over longer periods. A smaller longer-term gain in *SOC* of 15 g C m⁻² y⁻¹ (0–15 cm) was measured with radiocarbon dating by *Thuille et al.* [2000] during 200 years in dry grassland following conversion from forest in the Italian Alps.

6. Conclusions

[49] The effects of soil drying on grassland *GPP* were best modeled from the interaction of stomatal and nonstomatal effects of plant water status on CO₂ fixation. Both effects could

Table A1. List of Variables

Variable	Definition	Unit	Equation	Value	Reference
α	shape parameter for response of J to I	–	(5c)	0.8	Grant [1989]
β	stomatal resistance shape parameter	MPa ⁻¹	(2a, 2b)	5.0	Grant et al. [1999]
C_b	[CO ₂] in canopy air	$\mu\text{mol mol}^{-1}$	(1, 5a)		
C_c	[CO ₂] in leaf chloroplasts at ambient C_i	μM	(5b)		
C_i	[CO ₂] in leaf mesophyll at ambient ψ_c	$\mu\text{mol mol}^{-1}$	(5a)		
C_i'	[CO ₂] in leaves at $\psi_c = 0$ MPa	$\mu\text{mol mol}^{-1}$	(1)	0.67 C_b	Larcher [2001]
C_N	N:C ratio of M_b	g N g C ⁻¹	(11)		
C_N'	maximum N:C ratio of M_b	g N g C ⁻¹	(11)	0.22 ($j = \text{labile}$), 0.13 ($j = \text{resistant}$)	Grant et al. [1993a, 1993b]
C_P	P:C ratio of M_b	g P g C ⁻¹	(11)		
C_P'	maximum P:C ratio of M_b	g P g C ⁻¹	(11)	0.022 ($j = \text{labile}$), 0.013 ($j = \text{resistant}$)	Grant et al. [1993a, 1993b]
[DOC]	dissolved organic C concentration	g m ⁻³	(11)		
D_s	decomposition of S by M	g C m ⁻² h ⁻¹	(9)		
D_s'	Specific decomposition of S by M at 25°C and saturating S	g C g C ⁻¹ h ⁻¹	(10)		
D_s''	Specific decomposition of S by M at 25°C and ambient S	g C g C ⁻¹ h ⁻¹	(9, 10)		
e_a	Atmospheric vapor density at T_a and ambient humidity	g m ⁻³	(3)		
e_c	canopy vapor density at T_c and ψ_c	g m ⁻³	(3)		
\bar{A}	quantum yield	$\mu\text{mol e}^-$ $\mu\text{mol quanta}^{-1}$	(5c)	0.45	Farquhar et al. [1980]
f_N	nutrient effect on V_c	–	(5b)		
f_T	temperature effect on V_c	–	(5b)	Arrhenius	
f_{T_a}	temperature effect on R_c	–	(6)	Arrhenius	
f_{T_m}	temperature effect on D_s, R_h	–	(9, 11)	Arrhenius	
F_{ψ}	nonstomatal effect of ψ_i on V_c	–	(4, 5b)		
Γ	CO ₂ compensation point	μM	(5b)		
I	Irradiance	$\mu\text{mol m}^{-2} \text{s}^{-1}$	(5c)		
J	electron transport rate	$\mu\text{mol m}^{-2} \text{s}^{-1}$	(5b, 5c)		
J_{max}	electron transport rate at nonlimiting I, ψ_c, T_c and N,P	$\mu\text{mol m}^{-2} \text{s}^{-1}$	(5c)	400 $\mu\text{mol g chlorophyll}^{-1} \text{s}^{-1} \times \text{g chlorophyll m}^{-2}$	Farquhar et al. [1980]
K_c	Michaelis-Menten constant for carboxylation	μM	(5b)	12.5 at 25°C and zero O ₂	Farquhar et al. [1980]
K_{i_D}	inhibition constant for M_b on S during D_s	g C m ⁻³	(10)	25	Grant et al. [1993a, 1993b]
K_{m_D}	Michaelis-Menten constant for D_s	g C Mg ⁻¹	(10)	75	
$K_{m_{DOC}}$	Michaelis-Menten constant for R_h on [DOC]	g C m ⁻³	(11)	36	
M_b	heterotrophic microbial C	g C m ⁻²	(9, 10, 11)		
M_c	phytomass C	g C m ⁻²	(3)		
Ω_a	axial resistance to water transport along axes of primary ($x = 1$) or secondary ($x = 2$) roots or mycorrhizae	MPa h m ⁻¹	(3)		
Ω_r	Radial resistance to water transport from surface to axis of roots or mycorrhizae	MPa h m ⁻¹	(3)		
Ω_s	Radial resistance to water transport from soil to surface of roots or mycorrhizae	MPa h m ⁻¹	(3)		
θ_c	canopy water content	m ³ g C ⁻¹	(3)		
R_a	autotrophic respiration	g C m ⁻² h ⁻¹	(8)		
R_c	respiration of σ_c	g C m ⁻² h ⁻¹	(6, 7, 8)		
R_c'	specific respiration of σ_c at $T_c = 25^\circ\text{C}$	g C g C ⁻¹ h ⁻¹	(6)	0.015	Grant [1989]
R_h	heterotrophic respiration by M_b under ambient [DOC], O ₂ , nutrients, temperature	g C m ⁻² h ⁻¹	(11)		
R_h'	specific heterotrophic respiration by M_b under nonlimiting [DOC], O ₂ , nutrients, and 25°C	g C g C ⁻¹ h ⁻¹	(11)	0.15	Grant et al. [1993a, 1993b]
R_m	Maintenance respiration	g C m ⁻² h ⁻¹	(7)		
R_s	respiration of remobilized leaf or root C	g C m ⁻² h ⁻¹	(7, 8)		
r_a	Canopy aerodynamic resistance	s m ⁻¹	(3)		
r_c	canopy stomatal resistance	s m ⁻¹	(2b, 3)		
$r_{c\text{min}}$	canopy stomatal resistance at $\psi_c = 0$ MPa	s m ⁻¹	(2b)		
r_l	leaf stomatal resistance	s m ⁻¹	(2a, 4, 5a)		
$r_{l\text{max}}$	leaf cuticular resistance	s m ⁻¹	(2a)	5.0×10^3	Larcher [2001]

Table A1. (continued)

Variable	Definition	Unit	Equation	Value	Reference
r_{\min}	leaf stomatal resistance at $\psi_c = 0$ MPa	s m^{-1}	(1, 2a, 4)		
S	solid or sorbed organic C in soil	g C m^{-2}	(10)		
σ_c	nonstructural C	g m^{-2}	(6)		
$V_{b\max}$	leaf carboxylation rate at nonlimiting CO ₂ , ψ_c , temperature and N,P	$\mu\text{mol m}^{-2} \text{s}^{-1}$	(5b)	$40 \mu\text{mol g rubisco}^{-1} \text{s}^{-1} \times \text{g rubisco m}^{-2}$	Farquhar et al. [1980]
V_c	canopy CO ₂ fixation rate at ambient ψ_c	$\mu\text{mol m}^{-2} \text{s}^{-1}$	(5a)		
V'_c	potential canopy CO ₂ fixation rate at $\psi_c = 0$ MPa	$\mu\text{mol m}^{-2} \text{s}^{-1}$	(1)		
Y	carboxylation yield	$\mu\text{mol CO}_2 \mu\text{mol e}^{-1}$	(5b)		
ψ_c	canopy water potential	MPa	(3)		
ψ_s	soil water potential	MPa	(3)		
ψ_t	canopy turgor potential	MPa	(2a, 2b)	$\psi_c - \psi_\pi$	
Subscripts		Definition			
i		plant species, soil microbe-substrate complex			
j		tiller or branch of plant species, kinetic component of soil microbe-substrate complex			
k		node of tiller or branch			
l		canopy or soil layer			
m		azimuth class of leaf in canopy layer			
n		inclination class of leaf in azimuth class, microbial functional type			
o		irradiance class of leaf in inclination class (sunlit or shaded)			
x		root order (primary or secondary)			
z		root or mycorrhizae			

be modeled as related functions of plant water status where nonstomatal effects were less limiting (e.g. equation (4)). Interaction between these effects was achieved by solving for the C_i at which the diffusion of gaseous CO₂ constrained by stomatal effects equaled the carboxylation of aqueous CO₂ constrained by nonstomatal effects (equation (5)). This interaction allowed declines in modeled GPP and C_i to follow those in GPP and C_i calculated from EC and $\delta^{13}C$ values during soil drying. Alternative parameterizations of nonstomatal effects to that in equation (4) caused a loss in the accuracy with which seasonal changes in GPP and C_i were modeled. The accurate simulation of these changes made an important contribution to the simulation of climate effects on grassland NEP by a comprehensive ecosystem model.

Appendix A

[50] A list of variables with definitions and units is given in Table A1.

[51] **Acknowledgments.** Computational facilities for *ecosys* were provided through the Western Canada Research Grid (Westgrid). Field studies and carbon isotope analyses were funded by grants from the Natural Sciences and Engineering Research Council of Canada.

References

- Anderson, D. W. (1977), Early stage of soil formation on glacial till mine spoils in a semi-arid climate, *Geoderma*, 19, 11–19.
- Ball, J. T., I. E. Woodrow, and J. A. Berry (1987), A model predicting stomatal conductance and its contribution to the control of photosynthesis under different environmental conditions, in *Progress in Photosynthesis Research*, edited by J. Biggens, pp. 221–224, Martinus Nijhoff, Dordrecht.
- Barr, A. G., T. A. Black, E. H. Hogg, N. Kljun, K. Morgenstern, and Z. Nestic (2004), Inter-annual variability in the leaf area index of a boreal aspen-hazelnut forest in relation to net ecosystem production, *Agric. For. Meteorol.*, 126, 237–255.
- Cowan, I. R. (1965), Transport of water in the soil-plant-atmosphere system, *J. Appl. Ecol.*, 2, 221–239.

- Doussan, C., G. Vercambre, and L. Pagès (1998), Modelling of the hydraulic architecture of root systems: An integrated approach to water absorption – distribution of axial and radial conductances in maize, *Ann. Bot.*, 81, 225–232.
- Ennahli, S., and H. J. Earl (2005), Physiological limitations to photosynthetic carbon assimilation in cotton under water stress, *Crop Sci.*, 45, 2374–2382.
- Falge, E., et al. (2005), Comparison of surface energy exchange models with eddy flux data in forest and grassland ecosystems of Germany, *Ecol. Model.*, 188, 174–216.
- Farquhar, G. D., S. von Caemmerer, and J. A. Berry (1980), A biochemical model of photosynthetic CO₂ assimilation in leaves of C₃ species, *Planta*, 149, 78–90.
- Farquhar, G. D., J. R. Ehleringer, and K. T. Hubick (1989), Carbon isotope discrimination and photosynthesis, *Ann. Rev. Plant Physiol. Plant Mol. Biol.*, 40, 503–547.
- Ferreira, R. A., J. L. Dardanelli, L. B. Pachepsky, D. J. Collino, P. C. Faustini, G. Giambastiani, V. R. Reddy, and J. W. Jones (2003), Non-linear effects of water stress on peanut photosynthesis at crop and leaf scales, *Ecol. Model.*, 168, 57–76.
- Flanagan, L. B., and B. G. Johnson (2005), Interacting effects of temperature, soil moisture and plant biomass production on ecosystem respiration in a northern temperate grassland, *Agric. For. Meteorol.*, 130, 237–253.
- Flanagan, L. B., L. A. Wever, and P. J. Carlson (2002), Seasonal and interannual variation in carbon dioxide exchange and carbon balance in a northern temperate grassland, *Global Change Biol.*, 8, 599–615.
- Garcia, R. L., S. P. Long, G. W. Wall, C. P. Osborne, B. A. Kimball, G. Y. Nie, P. J. Pinter Jr., R. L. LaMorte, and F. Wechsung (1998), Photosynthesis and conductance of spring-wheat leaves: field response to continuous free-air CO₂ enrichment, *Plant Cell Environ.*, 21, 659–669.
- Goldberg, V., and C. Bernhofer (2001), Quantifying the coupling degree between land surface and the atmospheric boundary layer with the coupled vegetation-atmosphere model HIRVAC, *Ann. Geophys.*, 19, 581–587.
- Gollan, T., J. B. Passioura, and R. Munns (1986), Soil water status affects the stomatal conductance of fully turgid wheat and sunflower leaves, *Aust. J. Plant Physiol.*, 13, 459–464.
- Grant, R. F. (1989), Test of a simple biochemical model for photosynthesis of maize and soybean leaves, *Agric. For. Meteorol.*, 48, 59–74.
- Grant, R. F. (1998), Simulation in *ecosys* of root growth response to contrasting soil water and nitrogen, *Ecol. Model.*, 107, 237–264.
- Grant, R. F., N. G. Juma, and W. B. McGill (1993a), Simulation of carbon and nitrogen transformations in soils. I. Mineralization, *Soil Biol. Biochem.*, 27, 1317–1329.
- Grant, R. F., N. G. Juma, and W. B. McGill (1993b), Simulation of carbon and nitrogen transformations in soils. II. Microbial biomass and metabolic products, *Soil Biol. Biochem.*, 27, 1331–1338.

- Grant, R. F., G. W. Wall, B. A. Kimball, K. F. A. Frumau, P. J. Pinter Jr., D. J. Hunsaker, and R. L. Lamorte (1999), Crop water relations under different CO₂ and irrigation: testing of ecosystems with the free air CO₂ enrichment (FACE) experiment, *Agric. For. Meteorol.*, *95*, 27–51.
- Grant, R. F., N. G. Juma, J. A. Robertson, R. C. Izaurralde, and W. B. McGill (2001), Long-term changes in soil carbon under different fertilizer, manure, and rotation: testing the mathematical model ecosys with data from the Breton plots, *Soil Sci. Soc. Am. J.*, *65*, 205–214.
- Grant, R. F., et al. (2004), How elevated CO₂ affects water relations, water use and growth of irrigated sorghum: testing a model with results from a Free Air CO₂ Enrichment (FACE) experiment, *Agron. J.*, *96*, 1693–1705.
- Grant, R. F., T. A. Black, E. R. Humphreys, and K. Morgenstern (2006a), Changes in net ecosystem productivity with forest age following clear-cutting of a coastal Douglas fir forest: testing a mathematical model with eddy covariance measurements along a forest chronosequence, *Tree Physiol.*, *27*, 115–131.
- Grant, R. F., et al. (2006b), Modelling water stress effects on CO₂ and energy exchange in temperate and boreal deciduous forests, *Ecol. Model.*, *196*, 289–312.
- Grote, R., F. Suckow, and K. Bellman (1998), Modelling of carbon-, nitrogen- and water-balances in Scots pine stands, in *Changes of Atmospheric Chemistry and Effect on Forest Ecosystems*, edited by R. F. Hüttl and K. Bellman, pp. 251–281, Kluwer Acad., Dordrecht, Netherlands.
- Grünhage, L., and H. D. Haenel (1997), PLATIN I: a model of plant-atmosphere interaction for estimating absorbed doses of gaseous pollutants, *Environ. Pollut.*, *98*, 37–50.
- Herkelrath, W. N., E. E. Miller, and W. R. Gardner (1977), Water uptake by plants. II. The root contact model, *Soil Sci. Soc. Am. Proc.*, *41*, 1039–1043.
- Hui, D., and R. B. Jackson (2006), Geographical and interannual variability in biomass partitioning in grassland ecosystems: a synthesis of field data, *New Phytol.*, *169*, 85–93.
- Kellomaki, S., and K. Y. Wang (1996), Photosynthetic responses to needle water potentials in Scots pine after a four-year exposure to elevated CO₂ and temperature, *Tree Physiol.*, *16*, 765–772.
- Kimball, J. S., M. A. White, and S. W. Running (1997), BIOME-BGC simulations of stand hydrologic processes for BOREAS, *J. Geophys. Res.*, *102*, 29,043–29,051.
- King, A. W., W. M. Post, and S. D. Wullschlegel (1997), The potential response of terrestrial carbon storage to changes in climate and atmospheric CO₂, *Clim. Change*, *35*, 199–237.
- Klumpp, K., et al. (2005), Large daily variation in ¹³C-enrichment of leaf-respired CO₂ in two *Quercus* forest canopies, *New Phytol.*, *167*, 377–384.
- Kramer, K., et al. (2002), Evaluation of six process-based forest growth models using eddy-covariance measurements of CO₂ and H₂O fluxes at six forest sites in Europe, *Global Change Biol.*, *8*, 213–224.
- Larcher, W. (2001), *Physiological Plant Ecology*, 4th ed., Springer, Berlin.
- Li, T., R. F. Grant, and L. B. Flanagan (2004), Climate impact on net ecosystem productivity of a semi-arid natural grassland: modeling and measurement, *Agric. For. Meteorol.*, *126*, 99–116.
- Lizama, H. M., and I. Suzuki (1990), Kinetics of sulfur and pyrite oxidation by *Thiobacillus thiooxidans*: Competitive inhibition by increasing concentrations of cells, *Can. J. Microbiol.*, *37*, 182–187.
- McGill, W. B., H. W. Hunt, R. G. Woodmansee, and J. O. Reuss (1981), Phoenix, a model of the dynamics of carbon and nitrogen in grassland soils, in *Terrestrial Nitrogen Cycles*, edited by F. E. Clark and T. Rosswall, *Ecol. Bull.*, *33*, 49–115.
- Mederski, H. J., L. H. Chen, and R. B. Curry (1975), Effect of leaf water deficit on stomatal and nonstomatal regulation of net carbon dioxide assimilation, *Plant Physiol.*, *55*, 589–593.
- Medrano, H., J. M. Escalona, J. Bota, J. Gulias, and J. Flexas (2002), Regulation of photosynthesis of C₃ plants in response to progressive drought: stomatal conductance as a reference parameter, *Ann. Bot.*, *89*, 895–905.
- Melillo, J. M., D. O. Hall, and G. I. Agren (1996), Executive summary, in *Global Change: Effects on Coniferous Forests and Grasslands*, edited by A. I. Breymeyer et al., pp. 9–11, John Wiley, Hoboken, N. J.
- Meyers, T. P. (2001), A comparison of water and CO₂ fluxes over rangeland for well-watered and drought conditions, *Agric. For. Meteorol.*, *106*, 205–214.
- Moncrieff, J. B., et al. (1997), A system to measure surface fluxes of momentum, sensible heat, water vapour and carbon dioxide, *J. Hydrol.*, *188–189*, 589–611.
- Nikolov, N. T. (1997), Mathematical modeling of seasonal biogeophysical interactions in forest ecosystems, Ph.D. thesis, Colorado State Univ., Fort Collins.
- Novick, K. A., P. C. Stoy, G. G. Katul, D. S. Ellsworth, M. B. S. Siqueira, J. Juang, and R. Oren (2004), Carbon dioxide and water vapor exchange in a warm temperate grassland, *Oecologia*, *138*, 259–274.
- Penning de Vries, F. W. T. (1982), Crop production in relation to availability of nitrogen, in *Simulation of Plant Growth and Crop Production*, edited by F. W. T. Penning de Vries and H. H. van Laar, pp. 213–221, Cent. for Agric. Publ. and Doc., Wageningen, Netherlands.
- Ponton, S., L. B. Flanagan, K. P. Alstad, B. G. Johnson, K. Morgenstern, N. Klujn, T. A. Black, and A. G. Barr (2006), Comparison of ecosystem water use efficiency among Douglas-fir forest, aspen forest and grassland using eddy covariance and carbon isotope techniques, *Global Change Biol.*, *12*, 294–310.
- Richardson, A. D., et al. (2006), A multi-site analysis of random error in tower-based measurements of carbon and energy fluxes, *Agric. For. Meteorol.*, *136*, 1–18.
- Sauchyn, D. J., J. Stroich, and A. Beriault (2003), A paleoclimatic context for the drought of 1999–2001 in the northern Great Plains of North America, *Geog. J.*, *169*, 158–167.
- Saxton, K. E., W. J. Rawls, J. S. Romberger, and R. I. Papendick (1986), Estimating generalized soil-water characteristics from texture, *Soil Sci. Soc. Am. J.*, *50*, 1031–1036.
- Schulze, E.-D. (1993), Soil water deficits and atmospheric humidity as environmental signals, in *Water Deficits: Plant Responses from Cell to Community*, edited by J. A. C. Smith and H. Griffiths, pp. 129–145, BIOS Sci., Oxford, UK.
- Stitt, M. (1991), Rising CO₂ levels and their potential significance for carbon flow in photosynthetic cells, *Plant Cell Environ.*, *14*, 741–762.
- Suyker, A. E., S. B. Verma, and G. G. Burba (2003), Interannual variability in net CO₂ exchange of a native tallgrass prairie, *Global Change Biol.*, *9*, 255–265.
- Tardieu, F., and W. J. Davies (1993), Root-shoot communication and whole-plant regulation of water flux, in *Water Deficits: Plant Responses from Cell to Community*, edited by J. A. C. Smith and H. Griffiths, pp. 147–162, BIOS Sci., Oxford, UK.
- Thuille, A., N. Buchmann, and E. D. Schulze (2000), Carbon stocks and soil respiration rates during deforestation, grassland use and subsequent Norway spruce afforestation in the Southern Alps, Italy, *Tree Physiol.*, *20*, 849–857.
- Tuzet, A., A. Perrier, and R. Leuning (2003), A coupled model of stomatal conductance, photosynthesis and transpiration, *Plant Cell Environ.*, *26*, 1087–1096.
- Twine, T. E., et al. (2000), Correcting eddy-covariance flux underestimates over a grassland, *Agric. For. Meteorol.*, *103*(3), 279–300.
- Wang, Y. P., and P. G. Jarvis (1990), Description and validation of an array model – MAESTRO, *Agric. For. Meteorol.*, *51*, 257–280.
- Wever, L. A., L. B. Flanagan, and P. J. Carlson (2002), Seasonal and interannual variation in evapotranspiration, energy balance and surface conductance in northern temperate grassland, *Agric. For. Meteorol.*, *112*, 31–49.
- White, E. M., E. R. Krueger, and R. A. Moore (1976), Changes in total N, organic matter, available P, and bulk densities of a cultivated soil 8 years after tame pastures were established, *Agron. J.*, *68*, 581–583.
- Williams, M., E. B. Rastetter, D. N. Fernandes, M. L. Goulden, S. C. Wofsy, G. R. Shaver, J. M. Melillo, J. W. Munger, S.-M. Fan, and K. J. Nadelhoffer (1996), Modeling the soil-plant-atmosphere continuum in a Quercus-Acer stand at Harvard Forest: the regulation of stomatal conductance by light, nitrogen and soil/plant hydraulic properties, *Plant Cell Environ.*, *19*, 911–927.
- Williams, M., Y. Malhi, A. D. Nobre, E. B. Rastetter, J. Grace, and M. G. P. Pereira (1998), Seasonal variation in net carbon exchange and evapotranspiration in a Brazilian rain forest: a modelling analysis, *Plant Cell Environ.*, *21*, 953–968.
- Zhai, T., R. H. Mohtar, H. D. Karsten, and M. Carlassare (2004), Modeling growth and competition of a multi-species pasture system, *Trans. ASAE*, *47*(2), 617–627.
- Zhang, Y., R. F. Grant, L. B. Flanagan, S. Wang, and D. L. Versegny (2005), Recent developments and testing of a carbon-coupled Canadian land surface scheme in a water-stressed northern temperate grassland, *Ecol. Model.*, *181*, 591–614.
- Zur, B., and J. W. Jones (1981), A model for the water relations, photosynthesis and expansive growth of crops, *Water Resour. Res.*, *17*, 311–320.

L. B. Flanagan, Department of Biological Sciences, University of Lethbridge, Lethbridge, AB, Canada T1K 3M4.

R. F. Grant, Department of Renewable Resources, University of Alberta, Edmonton, AB, Canada T6G 2E3. (robert.grant@afhe.ualberta.ca)